CHAPTER IV

SYNTHESIS, CHARACTERIZATION OF 1-BUTYL-4-METHYLPYRIDINIUM LAURYL SULFATE AND ITS INCLUSION PHENOMENON WITH β-CYCLODEXTRIN FOR ENHANCED APPLICATIONS

4.1. Introduction

Ionic liquids (ILs) have attracted much attention at present due to their unique physicochemical traits such as considerable ionic conductivity and formidable catalytic property. [1-4] Solution properties, as well as the host-guest inclusion complex the ionic liquids, biologically active molecules with molecular host e.g. cyclodextrin, were extensively studied by Roy et. al. [5-9] Inclusion complex of β-CD with ionic liquid surfactant had also been studied by Yan'an Gao and his co-workers. [10]

Imidazolium and pyrrolidinium-based ionic liquids were derived from conventional anionic surfactant sodium lauryl sulfate and their physicochemical properties were studied thoroughly by Jingjing Jiao et. al. [11] The Critical micelle concentration(CMC) value comparison of two derived ionic liquid-based surfactants, it was established that the CMC value of imidazolium ionic liquid based surfactant was lesser than pyrrolidinium based surfactant; again both were much lesser than the precursor sodium lauryl sulfate. Therefore if we can replace the ionic head part by the more hydrophobic organic charge group then resulting product would be a much better surface active agent, this was the underlying concept of the synthesis work.

Conjugation of pyridinium ionic liquid and anionic surfactant sodium lauryl sulfate in equimolar ratio can give a benign model system, which is still unavailable in the literature. This type of system would be neoteric & environmentally friendly as the precursor ionic liquid is also benign to nature as well as removal of metal ion involved in the strategic preparative methodology [12-14] and also made halogen-free to make it environmentally affectionate. [15]

There will be a chance of competitive & mixed inclusion which might give some new insight of supramolecular recognition within the solution which was seldom available in the related literature. Surfactant ability with this special type of inclusion also gives some interesting and important information with specific application. Pyridinium ionic liquid which was used as the precursor is a bulkier aromatic counterion than even imidazolium ion and expected to show more effectiveness than the former as surfactant [11]. This ionic liquid based surfactant is expected to have more comprehensive applications in many fields, such as materials science, drug delivery, and supramolecular science. [16] Sodium lauryl sulfate & β-CD (β-Cyclodextrin) containing vesicle was previously used to transport protein (peptide) hormone with high encapsulation capacity. The insulin-loaded vesicle was shown high physical stability and protects insulin from proteolytic degradation where the Sodium lauryl sulfate was used as the anionic surfactant. [17]

The outcome of the fluorimetric measurement of J. W. Park had proposed the formation of the 2:1 (β-Cyclodextrin-surfactant) complexes with alkane sulfonates and alkyl sulfates with chain length equal or greater than 10 & 8 respectively, [18] but the details study as well as the spectroscopic and microscopic information and related evidence of the previously mentioned (β-CD-surfactant) inclusion complexes was quite rare in the literature. Similarly, such counterion modified surfactant, quite similar to ion-pair amphiphile and their inclusion complex with Cyclodextrin is also quite unavailable in latest literature.

In the present work we have synthesized the 1-butyl-4-methylpyridinium lauryl sulfate by simple ion exchange technique from sodium lauryl sulfate and 1-butyl-4-methylpyridinium chloride; and characterized by UV-Vis, FTIR, NMR, and Mass spectroscopy (ESI-MS). The CMC value, host-guest inclusion complex of the synthesized product has been studied. Other thermodynamic parameters were also derived by various techniques. The Host Guest inclusion complex with β-CD has been studied with the help of conductivity, surface tension, UV-Vis, FTNMR, Refractive index (RI) and fluorescence study. The nature of the Host-Guest inclusion complex with β-CD was further justified and characterized by HR-TEM, which given a new and mixed mode supramolecular recognition pattern.

4.2. Experimental Section

4.2.1. Materials

1-Butyl-4-methylpyridinium chloride (BMPyCl), Sodium lauryl sulfate (SLS) have been used for synthesis. Double distilled water specific conductance 1 μS/cm, pH ~6.7–7.0 was used for all experimental purposes. The probe used for the fluorescence was Pyrene. The source and purity of the chemicals have been given table S.9.

4.2.2. Preparation

Before the start of the synthesis work, the solubility of the chosen precursor ILs and SLS have been precisely checked in the different solvent and finally dichloromethane (DCM) was chosen as a suitable solvent. The 1-butyl-4-methylpyridinium lauryl sulfate [BMPy] [LS] was prepared by simple ion exchange reaction of 1-butyl-4-methylpyridinium chloride [BMPy]Cl and sodium lauryl sulfate [SLS]. The precursor 1-butyl-4-methylpyridinium chloride and sodium lauryl sulfate in 1:1 molar ratio was taken in DCM and continuously stirred at room temperature for 5 hours. As the by-product precipitate was ionic in nature so it was in the solid state in the organic solvent, was removed by filtration. Then the immiscible phase was washed with water very gently until the phase becomes chloride-free (the presence of the chloride was tested by $AgNO_3$ in acidic solution). Used volatile solvent (DCM, boiling point 39.6°C) was removed gently by maintaining required temperature by a rotary evaporator. The product was dried, stored in dark place and vacuum desiccators for 72 hours. The aqueous solution which was used for chloride removal was also stored to check any product accumulation in the water, has been found negligible accumulation.

4.2.3. Apparatus and procedure

Fourier transform Infrared spectra (FTIR) were recorded in KBr pellets & ethanol with a PerkinElmer FT-IR spectrometer (RX-1) operating in the region of 4000 to 400 cm^{-1} at ambient temperature. [19]

^1H Nuclear magnetic resonance (NMR) experiments were performed in Bruker AVANCE spectrometer operating at 300 MHz frequency. [20] 400 MHz Bruker AVANCE spectrometer was used for inclusion complex study (^1H and 2D NOESY). The respective solutions were made in D_2O, data was reported as a chemical shift. [21]

Ultraviolet-visible (UV-Visible) spectra were recorded by JASCO V-530 UV/VIS Spectrophotometer, with an uncertainty of wavelength resolution of ±2 nm. The measuring temperature was controlled by an automated digital thermostat. [21]

High-Resolution Transmission Electron Microscopy (HRTEM) images were obtained with a Jeol JEM 2100 microscope operating at an accelerating voltage of 200 kV. The spot size availability in TEM mode was 20 to 200 nm. A drop of the sample solution (EtOH as dispersant) was added to a Formver™ 200 mesh copper mess support grid coated with the carbon film. The excess sample was manually blotted carefully with a Whatman 42 filter paper for 2 s. The grid was dried at 333.15 K for around 1 h before experimentation. Humidity during the experiment was 50-60%. In order to provide better contrast, uranyl acetate staining was used. [22]

The Conductance measurements were accomplished in a Mettler Toledo Seven Multi conductivity meter with uncertainty 1.0 μS m^{-1}, bearing a cell constant of about (0.1 ± 0.001) cm^{-1}. Temperature of the solutions were maintained to within = (298.15± 0.01) K using Brookfield Digital TC-550 temperature thermostat bath. The used cell was calibrated using a 0.01 M aqueous KCl solution. The uncertainty in temperature was ±0.01 K. [21]

Surface tension experiments were carried out by a platinum ring detachment method using a Tensiometer (K9, KRÜSS, Germany) at the experimental temperature. The accuracy of the surface tension measurement was within 0.1 mN m^{-1}. The constant temperature was maintained during the experiments with Remi ultra thermostat (CB-700) with precision 0.1K. [23]

Refractive index (RI) was measured with the help of a digital refractometer of Mettler Toledo Refracto 30GS. The light source was LED, λ=589.3 nm. The refractometer was calibrated using distilled water, and calibration was checked after every measurement. The uncertainty of the measurement was ± 0.0002 units. [24]

Steady-state fluorescence emission study was carried out in bench top spectrofluorimeter from photon technologies international (Quantamaster-40). [20]

Dynamic Light Scattering (DLS) was performed on a Zetasizer Nano ZS90 ZEN3690 light scattering apparatus (Malvern Instruments Ltd., Malvern, UK) with the He−Ne laser (632.8 nm, 4 mW) at a scattering angle of 90°. The temperature was maintained constant at 298.15 K. [25]

Electrospray ionization (ESI) mass spectrum measurement was done in the JEOL GCMATE II GC-MS with data system is a high resolution and double focusing instrument.

4.2.4. Characterization

FTIR analysis

The observed infrared frequencies of the bond of functional groups of both the precursor and product have been shown (Fig. S. 1. a) within the range of 500-4000 cm^{-1}. The IR spectra showing at 3439 cm^{-1} is ascribed to  bond stretching of quaternary amine (3330-3450 cm^{-1}) like structure of butylpyridinium ring due to ion pair formation with dodecyl sulfate. The peak at 3052 cm^{-1} is showing the stretching frequency of aromatic -C-H bond vibrations of pyridinium ring. The peaks of wave numbers of 2954cm^{-1} and 2851cm^{-1} are the aliphatic asymmetric and symmetric stretching (C-H) stretching vibration is due to the methyl group ($–CH_3$). The peaks at 2919 cm^{-1}, 1467 cm^{-1}, and 1380 cm^{-1} are for symmetric stretching, bending or deformation and wagging (umbrella mode) vibration respectively due to $-CH_2-$ group. Wave number 1643 cm^{-1} and 1605 cm^{-1} are due to C=C and C=N bond stretching vibration of pyridinium ring. The peak at wave number 806cm^{-1} is due to C-N stretching vibration. 1213 cm^{-1} and 1084 cm^{-1} is asymmetric stretching of $-SO_4^{-1}$(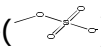), and symmetric stretching of $-SO_2-$ (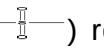) respectively. Peaks at 625 cm^{-1} and 581cm^{-1} are Pyridine in plane ring deformation. Based on FTIR analysis it was observed that synthesized ionic liquid was 1-Butyl-4-methylpyridinium lauryl sulfate [BMPy] [LS]. [26-34]

NMR analysis

The product [BMPy][LS] was characterized by ^1H NMR spectroscopy using D_2O and DMSO-d6 as a solvent on a spectrometer (Bruker Avance 300 spectrometer) for the determination of molecular structures and conformations. The ^1H NMR spectra data are shown in Fig. S. 2. a) and S. 2. b) in ppm (δ) from the internal reference (D_2O: δ 4.79ppm and DMSO-d6: δ 3.39ppm) in determining the proton chemical shifts.

The results of ^1H NMR of [BMPy][LS] are given as follows

^1H NMR (300 MHz, D_2O): δ 8.60-8.62(d, 2H, J=6.6 Hz) $N(CH)_2$ of pyridine, 7.80-7.83(d, 2H, J=6.3 Hz) $N^+CC(CH)_2$ of pyridine ring, 4.48(t, 2H, NCH_2), 3.89(t, 2H, $SOCH_2$,), 2.55 (s, 3H, $-CH_3$ para to N). 1.86 (m, 2H, $NCCH_2$), 1.55 (t,2H, $NCCCH_2$), 1.21 (m, $SOCH_2(CH_2)_9$, 20H), 0.80(m,3H, $NCCCCH_3$), 0.68(m,3H, $SOC_{11}CH_3$).

^1H NMR (300 MHz, DMSO-d6): δ 8.93-8.90(d, 2H, J=9Hz) $N(CH)_2$ of pyridine ring, 7.99-7.97(d, 2H, J=6 Hz) $N^+CC(CH)_2$ of pyridine ring, 4.54-4.51(t, 2H, NCH_2, J=4.5 Hz), 3.65(t, 2H, $SOCH_2$), 2.51 (s, 3H, $-CH_3$ para to N), 1.86 (m, 2H, $NCCH_2$), 1.46 (t, 2H, $NCCCH_2$), 1.24 (m, $SOCH_2(CH_2)_9$, 20H), 0.90(m,3H, $NCCCCH_3$), 0.85(m,3H, $SOC_{11}CH_3$).

Mass spectrum analysis

The calculated molecular weight of the product [BMPy][LS] was 403.41g.mol^{-1} and mass spectrum has confirmed the molecular ion peak (Fig. S. 3). The intense peak at 169.98 and 149.85 is due to n-dodecyl cation (primary carbocation) and 1-Butyl-4-methylpyridinium ion. The peak showing at 15, 57.12, 93.08, 96.06, and 136 is for methyl, n-butyl, 4-Methyl pyridinium, and 1-Butyl benzopyridinium ion respectively. Other probable peak assignments are like that 126.03 (Nonyl cation), 112.85(octyl ion), 98.41(heptyl cation), 92.02(4-methylpyridinium ion), 84.19(hexyl cation), 70.16(pentyl cation). Surface active agents usually suppress the electrospray ionization and [BMPy][DS] is itself a surface active agent.

UV-vis study

From the structure of the [BMPy][LS], it was quite clear that there was no chance of n-**π*** transition. Pyridinium ring with disturbed aromaticity having three conjugated double bonds. So we can expect UV band due to **π**-**π*** transition within the molecule. Two number of UV band appeared at 222 & 254 nm. The band of 222 nm was more intense than the 254 nm band.

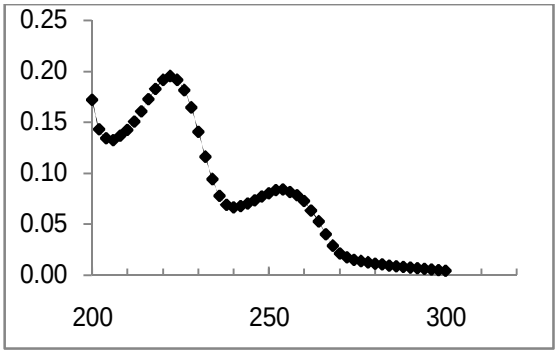

Fig.1 Absorption vs. wavelength graph in UV-VIS spectrum showing two characteristic bands at 222 and 254 nm respectively (0.003mM)

Results and Discussion

Study of Physicochemical Properties of [BMPy][LS]

4.3.1 Solubility test

The compound was soluble in the different organic solvent as well as enhanced water solubility compared to the precursor surfactant. The product obtained was performed the solubility test qualitatively.

Solvent	Water	$CHCl_3$	DMSO	DCM	CH_3OH	C_2H_5OH
Soluble	✓	✓	✓	✓	✓	Sparingly Soluble

(a)

Physical parameter with unit	Numerical value
N_{agg}	30
$\Delta\mu^0_{(M=1)}$ (J/mol)	-8500
β (L/mol)	20000
Γ_{max} (μmol/m^2)	5

(b)

Tab.1. (a): Solubility of [BMPy][LS] in different solvent

(b): Theoretically obtained physical quantity

4.3.2 Aggregation number

The average aggregation number (N_{agg}) is a fundamental and important parameter of micellar aggregation has been determined theoretically from STAND MODEL. [35] The aggregation number of [BMPy][LS] was found 30(Tab. 1.a.) is smaller than those of precursor SDS (N_{agg} =55). This was probably due to the larger size of the counter ion compared to the smaller size counter ion of the precursor. The negative value of the chemical potential ($\Delta\mu^0$, Gibbs free energy/mole) clearly indicates that the micellization process was thermodynamically controlled. This is also a clear indication for the product formation .[36] The interaction parameter (β) is In the L/mol unit. it's also important to mention that this model is best applicable to non-ionic surfactant. Therefore there would be some obvious deviation of the physical parameter if you apply this model to the case of the ionic surfactant like [BMPy] [LS].

4.3.3 Conductance study

The critical micelle concentration (CMC) is a narrow concentration range where the physical properties of the solution of an amphiphile show an abrupt change due to the cooperative formation of micelles in the bulk solution. [37] The CMC value can be obtained by the breakpoint of conductance curve and the dependence of physical properties was observed from there. The CMC value of sodium lauryl sulfate (SLS) was at 8 mM/dm^3. From the conductometric curve, (Fig. 2.b.) the CMC value of [BMPy] [LS] obtained at 1.53 mM. Therefore the [BMPy] [LS] compound has more efficient surface activity compared to its anionic surfactant (SLS). Upon reconsidering the result by the plot the molar [conductance] vs. [conc.] graph (Fig. 2. c.), the result would be more self-supporting. It had shown a breakpoint at around 1.52 mM.

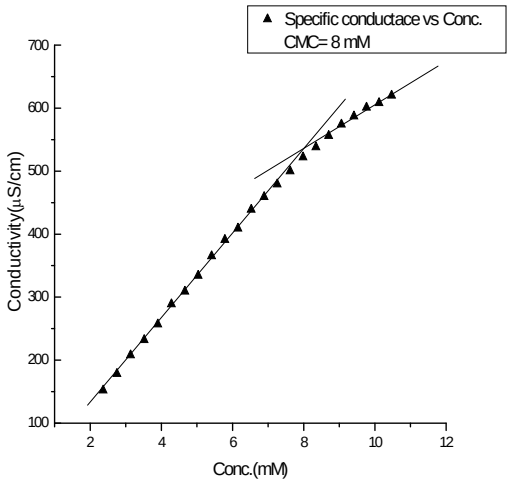

(a)

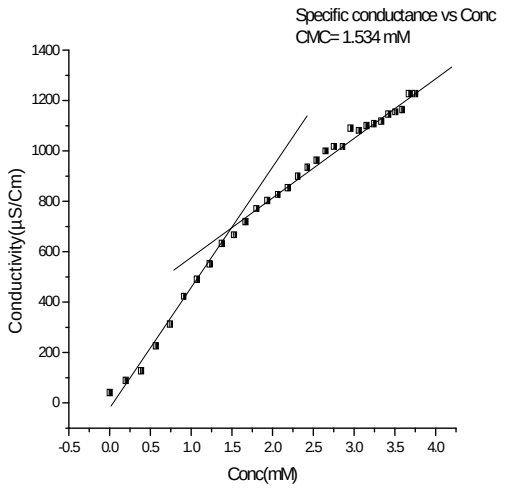

(b)

(c)

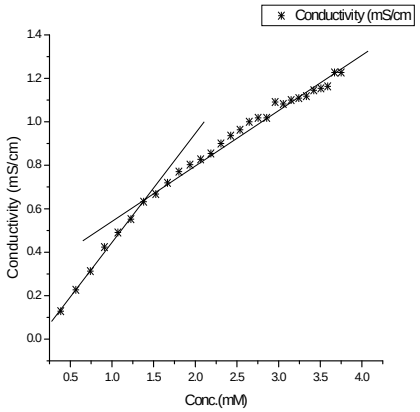

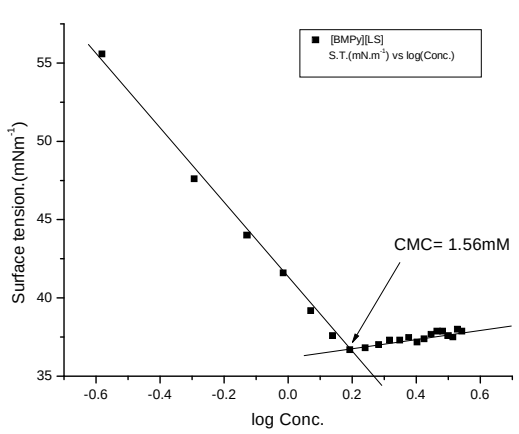

(d)

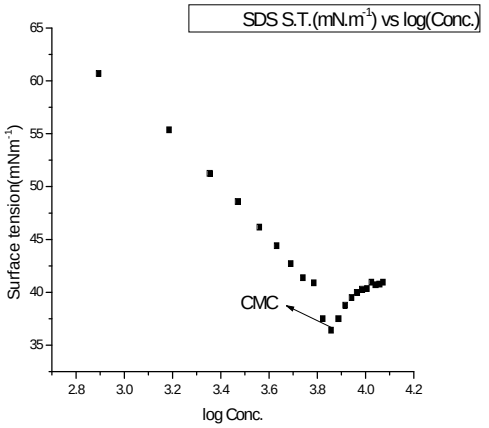

(e)

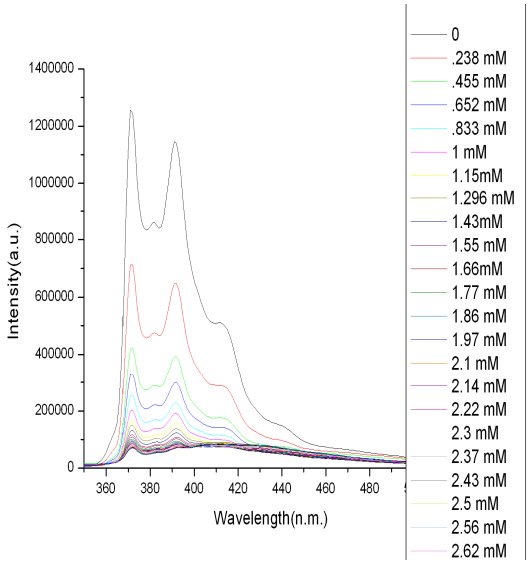

(f)

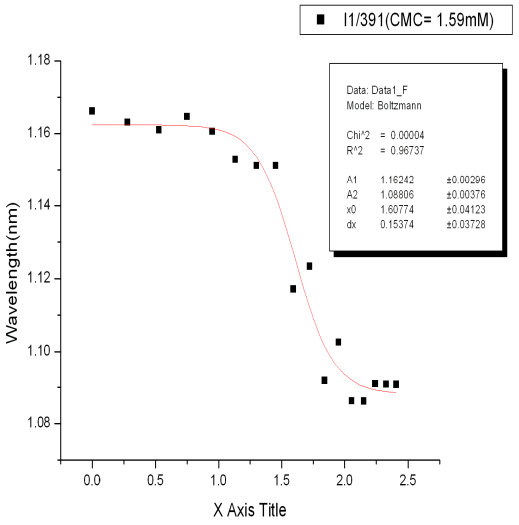

(g)

Fig. 2. a. b. The plot of conductance vs. conc. (mM) of SLS and [BMPy] [LS] respectively; c. The plot of molar conductance vs. conc. of [BMPy] [LS] d. Variation in the surface tension vs. log (conc.) of [BMPy] [LS] e. Variation in the surface tension with log (conc.) for SLS f. Steady-state Fluorescence spectra of [BMPy] [LS] g. Plot of the I1/I3 ratio of pyrene vs. conc. of [BMPy] [LS] for CMC

The fraction of the counter ions bound to the micelle has been evaluated by conductometry from the ratio of the post-micellar and premicellar slopes of the plot of molar conductivity vs. concentration curve (Fig.. 2.b.) of the surfactant solution. This fraction of the bound counter ions is represented by $f_b = m/n$ where m is the number of the counter ions bound per micelle and n is the aggregation number. The ratio of the post-micellar and premicellar

was around 0.51. On the other hand, the theoretical value of the aggregation number was 30, which was an approximate value.

The standard free energy of micellization per mole of the monomer unit (ΔG^{o}_{m}) for this system was evaluated by applying the equation.[38]

$$\Delta G^{o}_{m} = (1+ f_b)\ RT\ ln(CMC) \quad (1)$$

By putting the variables and constant in this equation the free energy of micellization per mole of the monomer unit of [BMPy][LS] was -39.28 Kjmol^{-1}.

4.3.4 Surface tension & surface parameters

The plot of surface tension with respect to the logarithm of concentration for [BMPy][LS] and SLS have been shown in Fig. 2. (d) & (e). From the breakpoint of the graph, the CMC value obtained by the surface tension measurement here is 1.56 mM, which was much lesser than precursor surfactant SLS. [37] The result is in good agreement with the conductance study.

The maximum surface excess concentration (Γ_{max}) and the minimum area of exclusion per molecule at the air-liquid interface (A_{min}) were estimated for the [BMPy][LS] from the inclination of the tensiometric profile near the CMC, is estimated by applying the Gibbs adsorption isotherm. [39] Two important parameters, i.e., saturation adsorption (τ_{max}) and minimum surface area per molecule (A_{min}) has been calculated from surface tension values using the following relationship [40-41]

$$\tau_{max} = 10^{23} / N_A \times A_{min} = -nRT\ (\partial\gamma / \partial \ln c)_T \quad (2)$$

For a dilute solution, the Gibbs equation could be expressed as [42]

$$-d\gamma = \Gamma_{exc}\, d\mu \quad (3)$$

Here γ and μ is the surface tension and the chemical potential respectively. Change in γ with the logarithm of surfactant concentration (c) can be used to determine the total surface excess as [43]

$$-d\gamma = RT\,\Gamma_{tot}\,d\ln C \quad (4)$$

Subsequently,

$$\Gamma_{tot} = -(1/RT)\,d\gamma/d\ln C \quad (5)$$

Here R and T are the universal gas constant and temperature in absolute scale respectively. The Γ_{tot} value near the CMC was termed as Γ_{max}. Thus,

$$\Gamma\,max = 1/2.303RT\,(-d\gamma/d\log C) \quad (6)$$

The value of the surface excess concentration for [BMPy][LS] was 4.91 µmol/m^2 (by the linear fitting of surface tension values before the CMC of [BMPy][LS] in Fig. 4. Using the surface excess value, A_{min} which represents the minimum area per surfactant molecule at the air-liquid interface has been estimated by the following relation [44]

$$A_{min} = 10^{18}/N_A\,\Gamma_{max} \quad (7)$$

The A_{min} value of [BMPy] [LS] in the aqueous system was found to be 0.34 nm^2 molecule^{-1}.

4.3.5 Fluorescence

The critical micellar concentration (CMC) of the anionic surfactant or identical species can be determined quite easily from the measurements of the fluorescence measurements in surfactant solution using polarity probe pyrene. [45]

The CMC measurement was done here by Steady-state fluorescence technique. Initially, blank pyrene solution was taken in the cuvette and surfactant containing pyrene solution was continuously added. From the graph, the value of CMC obtained is 1.56 mM (Fig. 2.f. & g.) which is quite close to the value 1.53 mM obtained from the conductance study.

Compound	cmc (mmol/L)	pC20	**γ**cmc (mN/m)	**A**min (nm^2)	**Γ**max (µmol/m^2)	**π**cmc (mN/m)
$[C_4mim][C_{12}SO_4]$[11 & 66]	1.80 ± 0.10 & 1.94	3.40 ±0.11	31.90 ±0.10	0.66 ±0.07	2.53± 0.27	40.30 ± 0.10
$[C_4MP][C_{12}SO_4]$[11 & 66]	2.70 ± 0.10 & 2.22	3.50 ±0.14	34.30 ± 0.10	0.74 ± 0.03	2.27 ± 0.08	37.9 ± 0.10

[BMPy][LS]	1.53 ± 0.10	-	36.50± 0.10	0.34	4.91	35.70± 0.10
[BMPy][LS] in presence of equimolar β-CD	-	-	33.80± 0.10	-	-	38.40± 0.10
C_{12}mimBr [46]	10.90	2.60	39.40	0.87	1.91	33.60
C_{12}MPB[47]	13.50	_	42.40	0.55	3.03	30.30
SDS[48 & 69]	7.80 & 7.90	2.40	39.60	0.48	3.45	32.50

Table 2. The comparison of different surface parameter of [BMPy][LS] alone & in presence of equimolar β-CD with some surfactants(Ionic liquid based surfactants, surface active ionic liquid and common anionic surfactant precursor).

[C_4mim][$C_{12}SO_4$] →1-Butyl-3-methylimidazolium dodecyl sulfate
[C_4MP][$C_{12}SO_4$] → N-Butyl-N-methylpyrrolidinium dodecyl sulfate

Inclusion phenomenon and microscopic morphology

4.4.1 From Conductance

Conductivity is a ingenuous method for studying the host-guest inclusion and it can be used to unravel whether the inclusion can occur [49, 50], also the stoichiometry of the host-guest inclusion complexes (ICs) formed. [51, 52]

Here the conductivity experiment was performed at some conventional concentration and also in the unparalleled concentration of the host and guest. It was a distinctive fact that the indicating breakpoint of the inclusion complexes (ICs) usually 5 times lesser than mother concentration of each solution. The experiment was carried out at two different concentrations of both the host as well as the guest e.g. 10 mM and 2 mM and the expected breakpoint was appear in 1.66 mM and 0.41(Fig. 3. a. & b.) mM of β-CD respectively also obtained experimentally. Another important point regarding the conductance graph was that(1st inclusion graph) except the breakpoint at 1.66 mM there also a breakpoint at 3.33, 5.1 mM thought it is not prominent like those at 1.66mM. So the inclusion stoichiometry of the host & guest may be both (1:1 & 2:1) or 1:2.

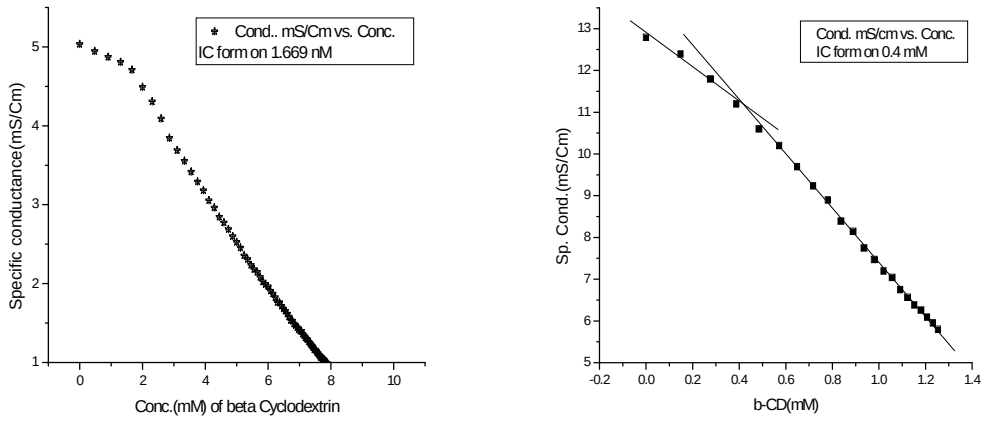

(a) (b)

Fig. 3 (a) Conductance vs. conc. (mM) of [BMPy][LS] & β-CD at 10 mM conc. of both (b) 2 mM of the both.

4.4.2 From Fluorescence

As already stated pyrene (polarity probe) I_1/I_3 method is helpful in determining the CMC of many surfactants. The surfactant [BMPy] [LS] itself was fluorescence inactive so its Host-Guest interaction with β-CD was preferably studied with the help of pyrene very briefly. The pyrene I_1/ I_3 ratio is very convenient and reliable method to find out the aggregation concentration which also helps to get an idea about the surrounding polarity around the probe molecule. If we carefully investigate the I_1 /I_3 ratio throughout the set of a solution it can be observed that in the presence of cyclodextrin only, it was more than 0.8 (I_1/I_3>0.8) (Fig. 4.). It's an indication of significant polarity around the pyrene molecules, probably due to free as well as some included pyrene molecule into the hollow cavity of cyclodextrin. Upon gradual increase of ([BMPy] [LS])'s concentration, the formation of inclusion complex increases and the pyrene I_1/I_3 ratio gradually decreases. These might be due to the preferable inclusion of a more hydrophobic group of [BMPy] [LS]), into the cage of cyclodextrin molecules which should gradually depart the pyrene from the host molecules.

It is also interesting to note that the set of solutions with more [BMPy][LS] concentration shows a gradual increase of I_1/I_3 ratio which may be due to excess concentration of the [BMPy][LS], provide some free long lipophilic chain may increases the polarity with respect to the pyrene. The solution with highest [BMPy][LS] concentration shows the maximum value of the ratio of first and third vibronic coupling due to the formation of aggregates with

a lipophilic core which encourages the pyrene molecule to enter that core, remaining sufficient but excess pyrene face the solution polarity. The I_1/I_3 ratio is the utmost in the higher concentration of [BMPy] [LS] with nearly zero concentration of β-cyclodextrin. It also needs to mention that this concentration is considerably greater than the CMC value of the surfactant [BMPy] [LS]. So this differential encapsulation of pyrene inside into the β-CD & [BMPy] [LS] may be used to separate analytically important but toxic pyrene.

Another important part of the fluorescence graph was a significant shift in the λmax position during the study. These bathochromic shifts appear after that set which had 1:1 molar ratio of the [BMPy] [LS] and cyclodextrin. This mixed concentration perhaps produces the initial occurrence of the inclusion which might be responsible for changes of solution thermodynamics and λmax.

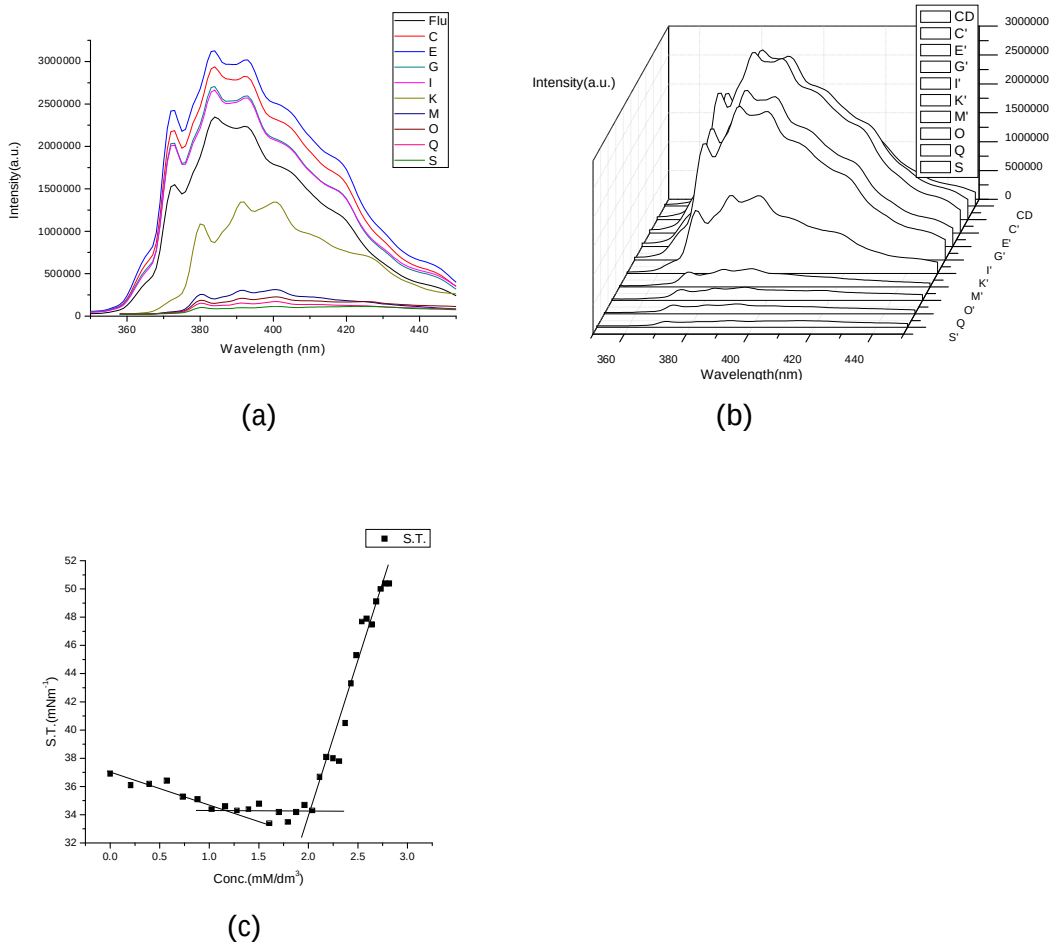

Fig. 4 (a) Fluorescence of pyrene in various concentrations of β-CD and ILBS (Gradual decrease in the conc. of β-CD & increase in the conc. of the ILBS) & (b) corresponding 3D plot. (c) The plot of the surface tension of [BMPy] [LS] vs. conc. (mM) of β-CD

Another pertinent finding was, pyrene fluorescence intensity was spectacularly reduced in the presence of [BMPy] [LS], which demands it may be used as the fluorescence quencher in fluorescent experiments. Many compounds containing the pyridinium ring usually being used as the probe as well as a quencher in the field of micellar and microemulsion research e.g. dodecyl, tetradecyl and hexadecyl attachment of the pyridinium ring. [53]

4.4.3 From surface tension

The surface tension graph had shown usual breakpoint along with some notability in the host-guest study. From the graph, it was clear that at 10 mM concentration of BuMPLS (much higher than the experimental CMC value) the minimum surface tension value was 37mNm^{-1} [Fig. 4 (c)]. In Sober fact for the utility of the inclusion, in this case, was the minimum surface tension value in the presence of β-CD was 34mNm^{-1}. This value was perfectly before the breakpoint for the inclusion. So it can be concluded that replacing the head group of the surfactant with the substituted pyridinium ring had enhanced surface activity which further can be ameliorated with the host β-Cyclodextrin. In the meantime, unintentional excess use and resulting loss of worthy and useful surfactant system can be avoided by the help of this systematic inclusion. Further β-CD can help in the controlled release of the surfactant, as well in its long term protection. The appearance of the multiple breakpoints also supports the possibility of inclusion other than 1:1 stoichiometry.

4.4.4 From UV-vis spectroscopy

Job's method is one of the peerless methods used to identify the stoichiometry of the host-guest inclusion complexes, known as the continuous variation method, which has been used here by using UV-visible spectroscopy. [54] A set of solutions for each [BMPy][LS] and β-CD was formulated varying the mole fraction (x) of the guest in the range x=0 to x=1. Job's plots were generated by plotting (x. ΔA versus mole fraction (x), where ΔA is the difference in absorbance of the [BMPy] [LS] without and with β-CD and x = [BMPy] [LS]/([BMPy][LS]+[β-Cyclodextrin]). [55-56] The x.ΔA vs. mole fraction (x) graph showed highest point at 0.50 if we consider the absorption maxima at 252 nm. The value of mole fraction (x) at the topmost deviation gives the stoichiometry of the inclusion complex (IC), *i.e.,* proportion of guest and host is 1:2 if x =0.33; 1:1 if x =0.5; and 2:1 if x =0.66 etc. In the present work also the value of maxima of job plot was found at R=0.367(near to 0.33) which suggest an approximate 2:1 stoichiometry (the absorption maxima at 220 nm) of the inclusion complexes [Fig. 5 (a) & (b)]. Most probably there was both the 1:1 & 2:1 inclusion. The alkyl chain of [BMPy] [LS]

form 2:1 inclusion with β-CD & pyridinium part probably make 1:1 inclusion was already assumed by T. Ray and her fellow colleagues. [57]

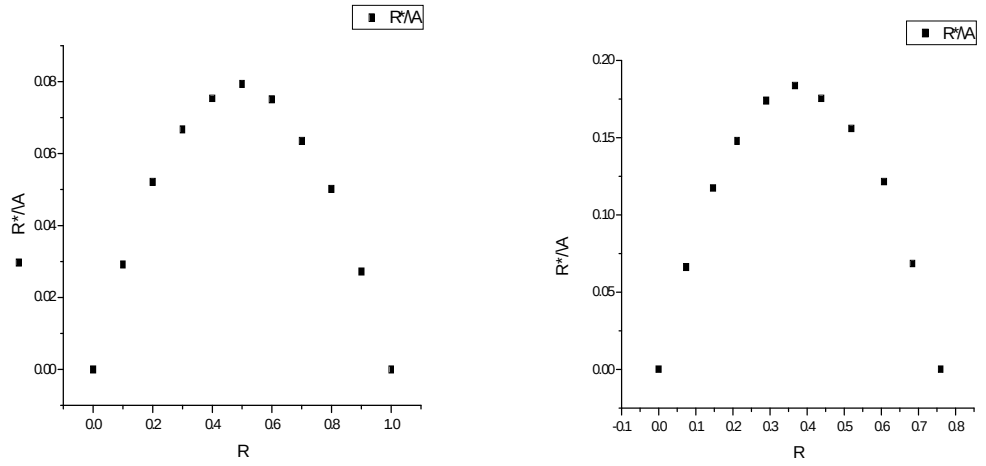

Fig.5. a) & b) Job's plot of [BMPy][LS]-β-CD systems at 298.15 K at λ max = 252 & 220 nm respectively.

4.4.5 From Refractive index: With the variation in concentration of [BMPy][LS]-β-CD system(Tab. S. 7) solution with highest and lowest β-CD concentration, the refractive index value was highest. This result was probably due to maximum inclusion & micellization with reverse equilibrium made the solution optically dense.

4.4.6 From NMR & 2D NOESY spectra: NMR is a very sensitive technique to establish the occurrence of inclusion as well as its mode. [58] The inclusion of a guest molecule inside into the cavity of β-CD results in the chemical shift of the interacting protons of both the guest and β-CD in 1H NMR spectra, due to their mutual screening through space. [59] Due to its unique truncated shape cyclodextrin cavity are non-uniform at the two side. The guest molecules usually like to approach the β-CD from the broader cone and as a result, the H1 & H3 undergoes the maximum shift in its δ values whereas H6 usually remains unaffected. [60] In our present study, we get a considerable shift in the δ value of H6 proton which again supports the formation of 2:1 inclusion. Other physicochemical techniques already gave the indication of both 1:1 & 2:1 inclusion which was further confirmed by UV-Vis Job plot & also by FTNMR [(Fig. S. 2. a, b); Fig. S. 6. a), b] Both the Pyridinium & dodecyl part of surfactant had shown in the shift of δ values which also confirm 1:1 & 2:1 mode of inclusion into the β-CD molecule. One of the most significant shift was observed for the singlet peak to the H (-CH_3 para to N of pyridinium ring). This was probably due to the symmetrical existing of -CH_3 group in between the narrower rim of the two cyclodextrin molecule, which

provides maximum shielding. The same condition may be probable in the case of 2:1 inclusion proposed by Ray et al. [57]

Two-dimensional (2D) NMR spectroscopy provides certain evidence about the spatial immediacy of the approaching atoms of the host and the guest by observing the intermolecular dipolar cross-correlations. Two protons are able to create a nuclear Overhauser effect (NOE) cross-correlation in NOE spectroscopy (NOESY) interacting through space, when they situated within 0.4 nm in space. [61-63]

2D NOESY showed correlation peak between **H1** [4.893-4.902 (H1, 7H, d)] proton of β-CD with NC**H**$_2$ of pyridinium ring [4.324-4.361(NC**H**$_2$, 2H, t)] (Fig. 6. B.). It may indirectly reject the possibility of the insertion of N(+)Butyl inside the β-CD cavity**.** There was significant cross peak between **H5, H6** [3.667-3.746 (H6, H5, 14H, m)] protons and **H1** proton [4.893-4.902 (H1, 7H, d)] of β-CD molecule (Fig. 6. B.). Probably upon inclusion β-CD molecules orient with each other in head to tail manner. A strong cross peak was obtained between **H1** proton and **H4** [3.441-3.66 (H4, 7H, t), proton of β-CD (Fig. 6. B.) molecule again strongly supports head to tail manner orientation of the β-CD. Here we able to see cross peaks between NC**H**$_2$ of pyridinium ring and between all other proton of β-CD (except **H1**), but weaker than those obtained with **H1**. One of the most important and interesting strong cross peak was between SOC**H**$_2$ 3.875-3.905(t, 2H, SOCH_2) of lauryl sulfate and between **H5, H6** [3.667-3.746 (H6, H5, 14H, m)] protons of the β-CD molecule (Fig. 6. B.) strongly suggests insertion of alkane chain through narrower cavity of the β-CD. This kind of insertion is only possible during 2:1 mode of inclusion. A very feeble cross peak between **H3** proton of β-CD [3.873-3.905(H3, 7H, t)] and NC**H**$_2$ of pyridinium ring [4.324-4.361(NC**H**$_2$, 2H, t)] said about (Fig. 6. B.) disfavor mode inclusion between broader β-CD cavity and butyl chain of the [BMPy][LS]**.** 2D NOESY at the aliphatic region also supports the inclusion complex formation. The cross peak between NCCC**H**$_2$ [(1.476-1.529) 2H, t] and SO(C**H**$_2$)$_{10}$ [(1.107-1.207)20H, m] (Fig. 6. C.) suggest disruption of micellar structure in the presence of inclusion complex.

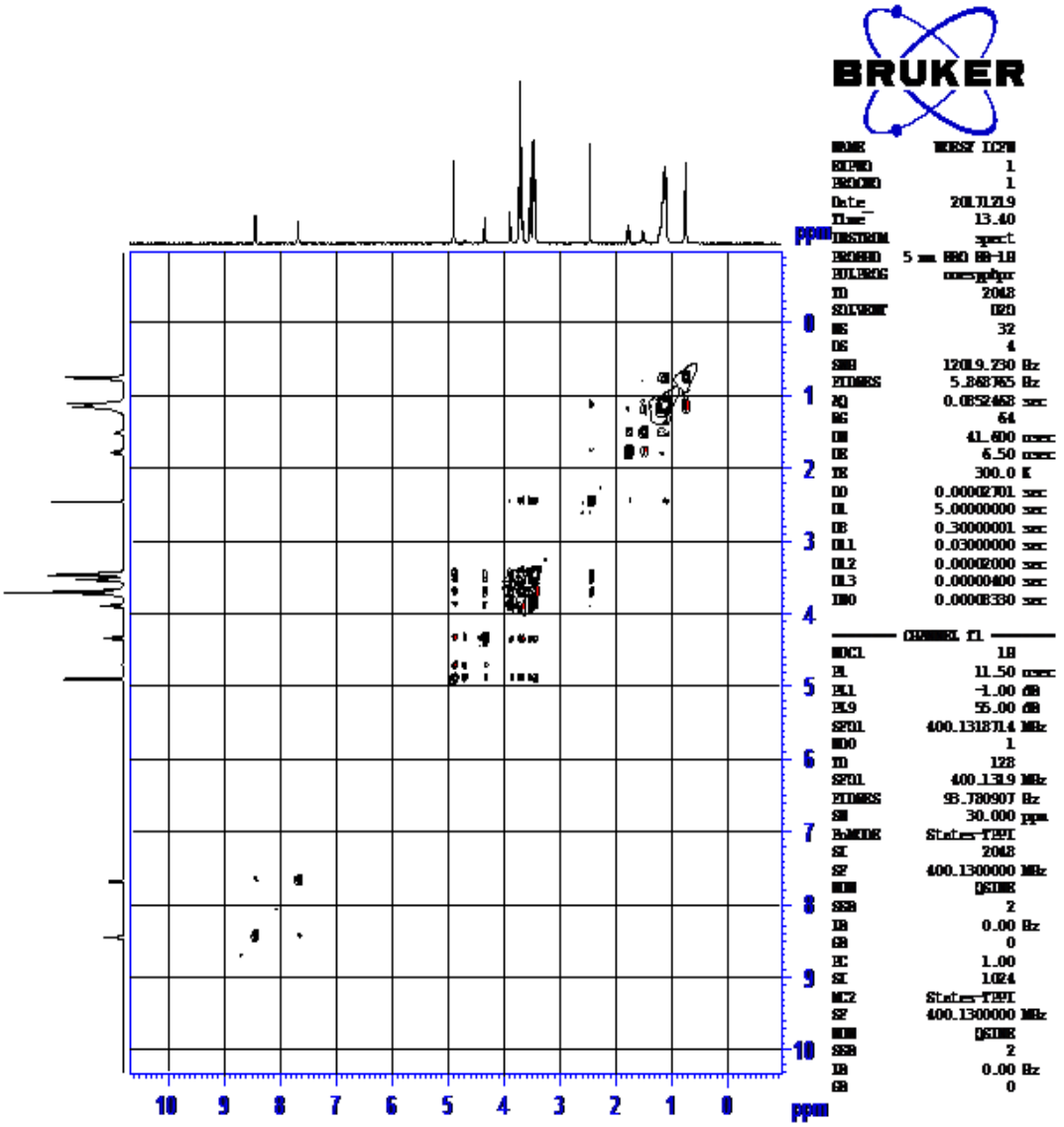

(a)

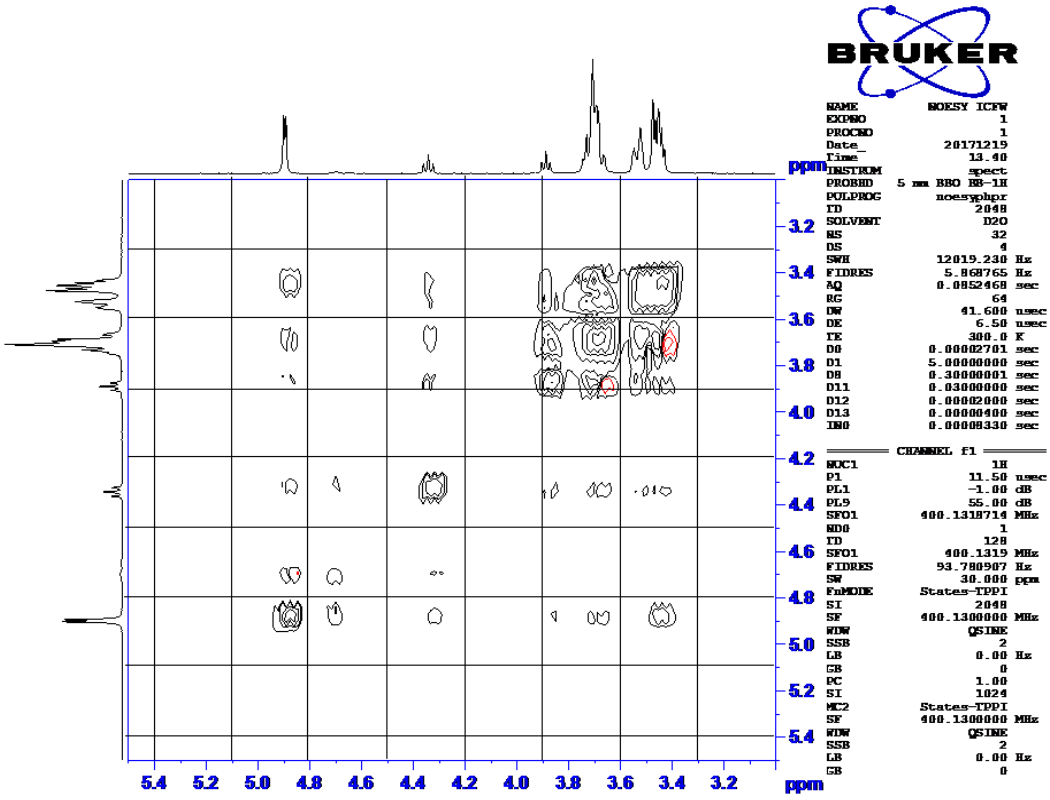
BRUKER
NAME NOESY ICFW
EXPNO 1
PROCNO 1
Date_ 20171219
Time 13.40
INSTRUM spect
PROBHD 5 mm BBO BB-1H
PULPROG noesyphpr
TD 2048
SOLVENT D2O
NS 32
DS 4
SWH 12019.230 Hz
FIDRES 5.868765 Hz
AQ 0.0852468 sec
RG 64
DW 41.600 usec
DE 6.50 usec
TE 300.0 K
D0 0.00002701 sec
D1 5.00000000 sec
D8 0.30000001 sec
D11 0.03000000 sec
D12 0.00002000 sec
D13 0.00000400 sec
IN0 0.00008330 sec
CHANNEL f1
NUC1 1H
P1 11.50 usec
PL1 -1.00 dB
PL9 55.00 dB
SFO1 400.1318714 MHz
ND0 1
TD 128
SFO1 400.1319 MHz
FIDRES 93.780907 Hz
SW 30.000 ppm
FnMODE States-TPPI
SI 2048
SF 400.1300000 MHz
WDW QSINE
SSB 2
LB 0.00 Hz
GB 0
PC 1.00
SI 1024
MC2 States-TPPI
SF 400.1300000 MHz
WDW QSINE
SSB 2
LB 0.00 Hz
GB 0
ppm
3.2
3.4
3.6
3.8
4.0
4.2
4.4
4.6
4.8
5.0
5.2
5.4
5.4 5.2 5.0 4.8 4.6 4.4 4.2 4.0 3.8 3.6 3.4 3.2
ppm

(b)

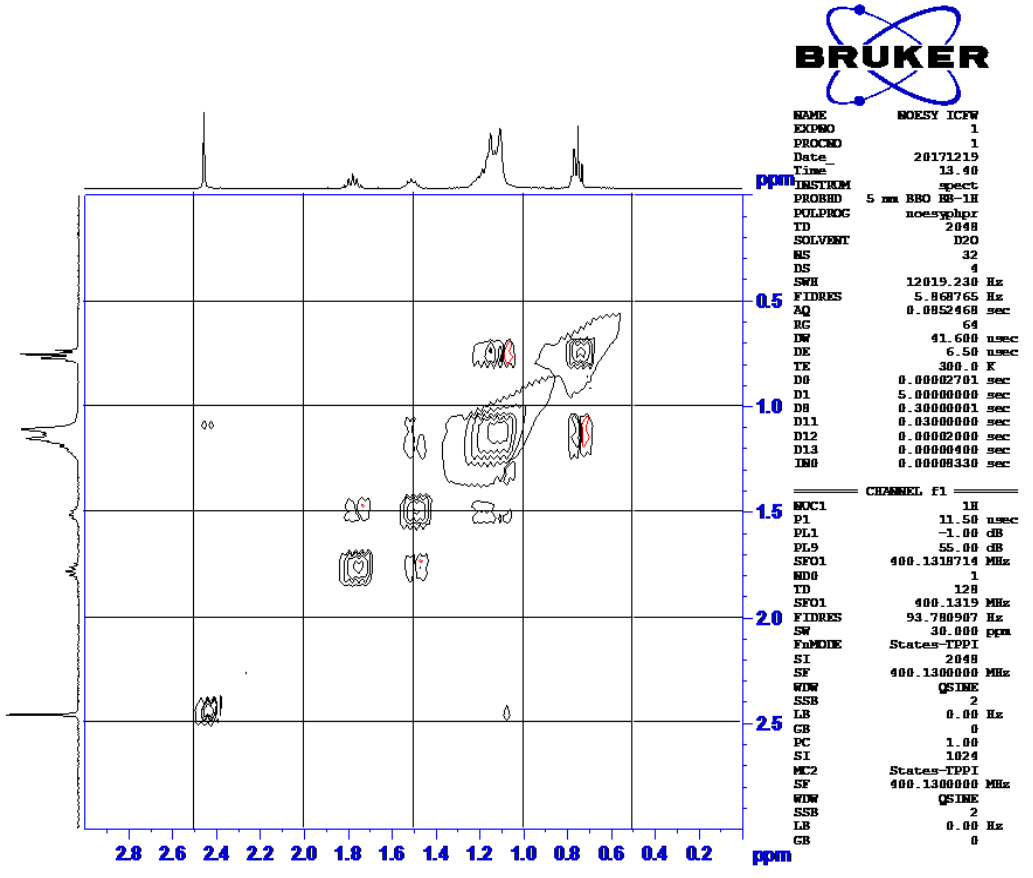
BRUKER
NAME NOESY ICFW
EXPNO 1
PROCNO 1
Date_ 20171219
Time 13.40
INSTRUM spect
PROBHD 5 mm BBO BB-1H
PULPROG noesyphpr
TD 2048
SOLVENT D2O
NS 32
DS 4
SWH 12019.230 Hz
FIDRES 5.868765 Hz
AQ 0.0852468 sec
RG 64
DW 41.600 usec
DE 6.50 usec
TE 300.0 K
D0 0.00002701 sec
D1 5.00000000 sec
D8 0.30000001 sec
D11 0.03000000 sec
D12 0.00002000 sec
D13 0.00000400 sec
IN0 0.00008330 sec
CHANNEL f1
NUC1 1H
P1 11.50 usec
PL1 -1.00 dB
PL9 55.00 dB
SFO1 400.1318714 MHz
ND0 1
TD 128
SFO1 400.1319 MHz
FIDRES 93.780907 Hz
SW 30.000 ppm
FnMODE States-TPPI
SI 2048
SF 400.1300000 MHz
WDW QSINE
SSB 2
LB 0.00 Hz
GB 0
PC 1.00
SI 1024
MC2 States-TPPI
SF 400.1300000 MHz
WDW QSINE
SSB 2
LB 0.00 Hz
GB 0
ppm
0.5
1.0
1.5
2.0
2.5
2.8 2.6 2.4 2.2 2.0 1.8 1.6 1.4 1.2 1.0 0.8 0.6 0.4 0.2
ppm

(c)

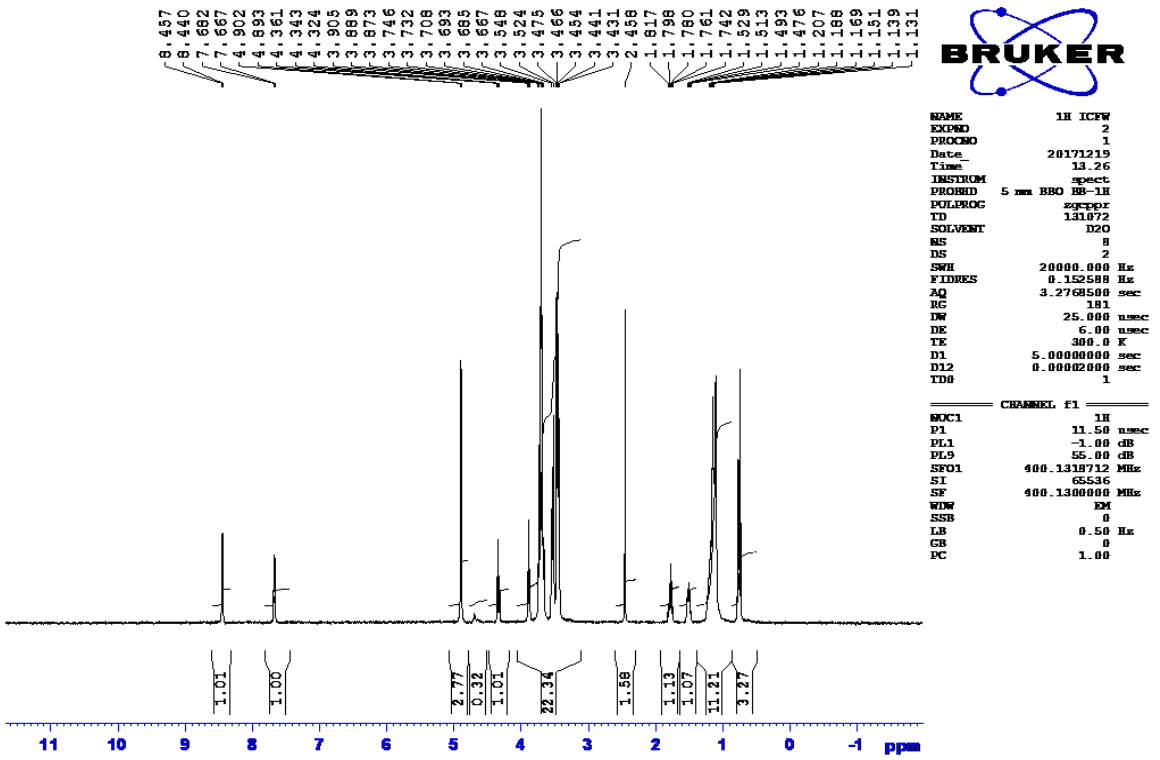

Fig.6. (a) 2D-NOESY spectrum of [BMPy] [LS]+ [β-Cyclodextrin] inclusion complex (excluding aromatic part).

(b) Extended part of the region enriched with β-CD peaks of the same.

(c) Extended part of the region enriched with aliphatic peaks of the [BMPy] [LS] + [β-Cyclodextrin] inclusion complex.

(d) ^{1}H NMR spectrum of [BMPy] [LS]+ [β-Cyclodextrin] inclusion complex for getting 2D NOESY.

4.4.7 From DLS: In DLS the size distribution of molecules or particles is the property of significance. Here, the distribution explains how much material there is nearby of the different size "slices." In DLS, the local distribution is the concentration distribution which indicates how much light is scattered from the various size "slices" or "bins." Historically, a simpler forced single exponential fitting method (the cumulant method) has been used to find an overall mean size (by intensity) and an overall polydispersity (the normalized next cumulant). Traditionally, this overall polydispersity has also been converted into an overall polydispersity index PDI which is the square of the light scattering polydispersity. For a perfectly uniform sample, the PDI would be (0.0). We had obtained the average PDI value of 0.711 which indicate broad poly dispersity of the inclusion complex, supported by HRTEM. [64-65] If only 1:1 inclusion complex were formed, and then the values of PDI (Table S.10) for this system should be less than 0.50 consistently, is usually due to the homogeneous

distribution of the host-guest systems. Therefore light scattering tool indirectly but strongly support the formation of both 1:1 and 2:1 mode of inclusion.

4.4.8 From HRTEM: To visualize the structural modification at the microscopic level the solution was taken in the moderate concentration for both the (β-Cyclodextrin) & its inclusion complex (Fig. 7. & 8). The High resolution transmission electron microscopy (HRTEM) images of β-CD were classic in nature. The occurrence of the 2:1 inclusion was confirmed from the vesicle type of structure obtained from HRTEM, as such bulkier morphology is possible only when the 2:1 inclusion complex is formed. Large amounts of spherical poly-disperse aggregates ranging from 50 to 445 nm in diameter was found, which were certified to be hollow vesicles rather than solid spheres. This also an indication of dynamic equilibrium previously proposed [57] also prove possibilities of other another mode of inclusion as shown in scheme 1 & assumed earlier by Li et al. [17] The few inconsistencies with the DLS size may be accounted for by noting that HRTEM and DLS show solid and swollen vesicles, correspondingly. [66] So the formation of vesicles due to 2:1 inclusion was proved with direct evidence namely HRTEM, only the presence of micelle of homogeneous 1:1 inclusion complex can't produce such broader morphology alone. [67, 68]

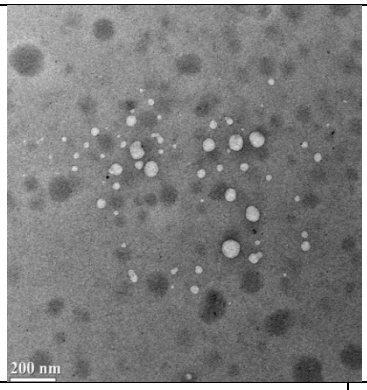

1

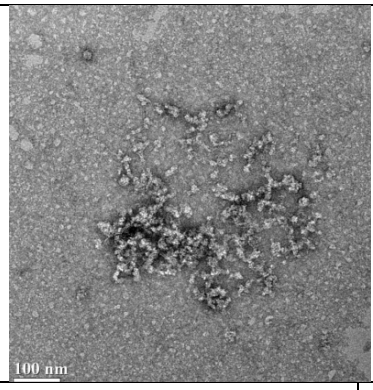

2

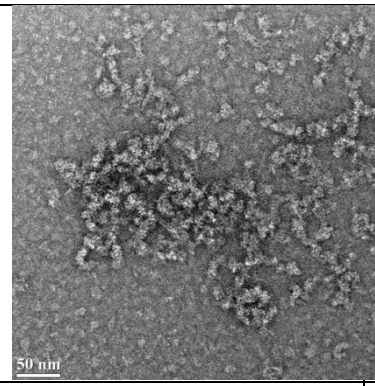

3

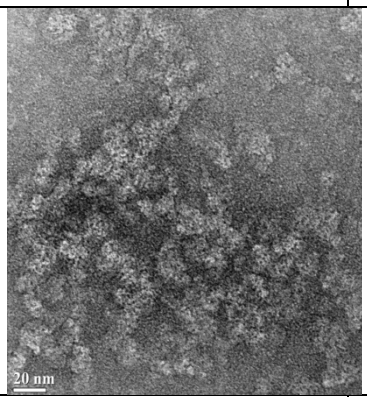

4

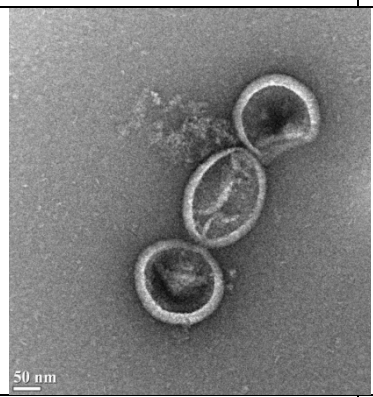

5

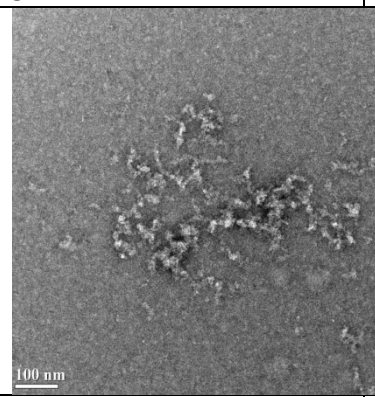

6

Fig. 7.: TEM representation of β-CD at 1) Different size structure are spread out with maximum size within 100 nm 2) Typical morphology of β-CD (100 nm scale) 3) Usual texture of β-CD (50 nm scale) 4) Morphology of β-CD at high resolution (20 nm reference scale) 5) Distinct shape with unique morphology 6) Dispersed appearance with average size quite comparable to obtained from the DLS.

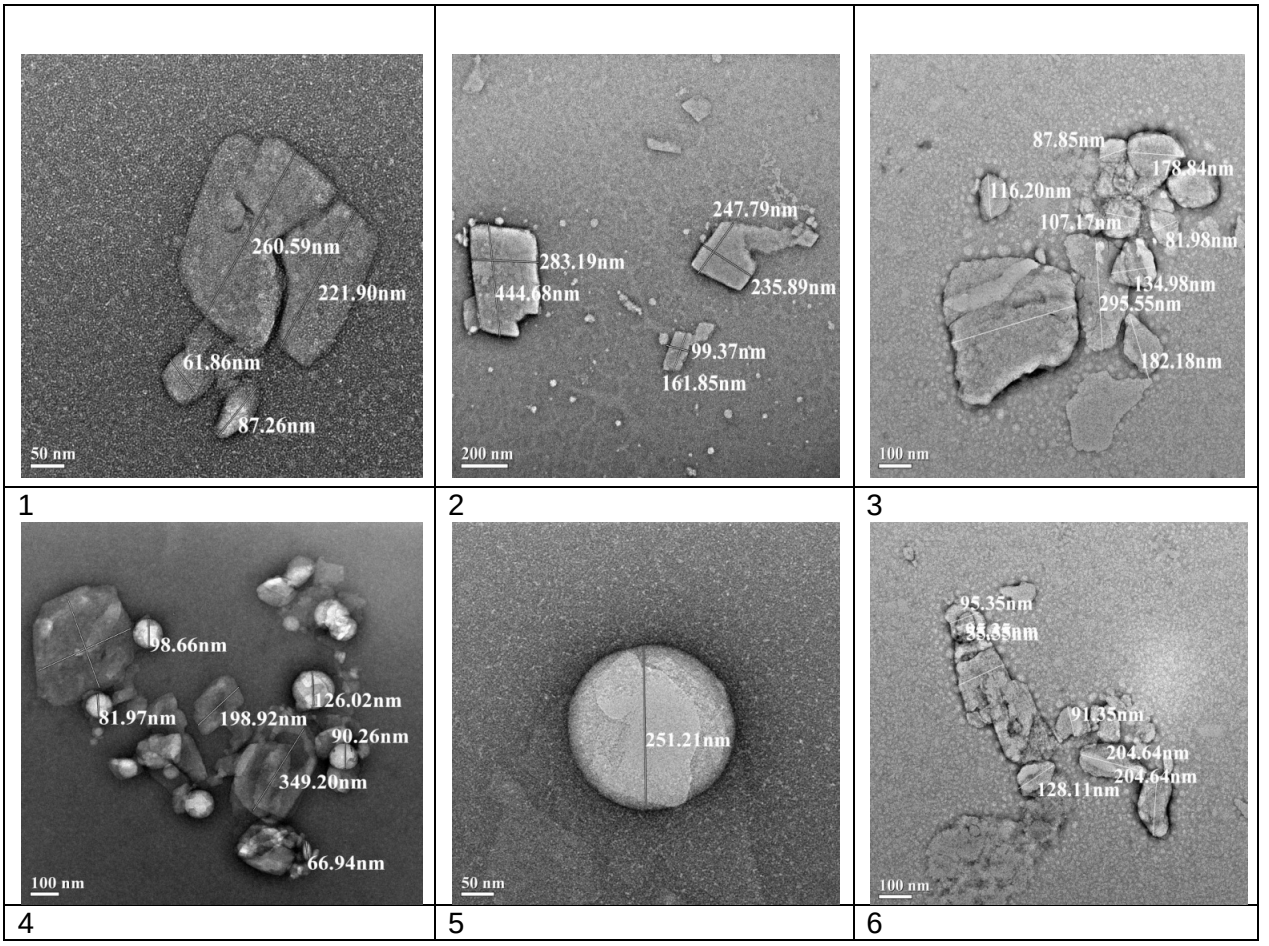

Fig. 8.: TEM representation of β-CD+ [BMPy][LS] inclusion complex at 1) Aggregated form with two smaller out growths 2) Randomly aggregated structure with 200 nm scale, probably of inclusion complex 3) Cluster of different sizes structure 4) Medium size vesicle with non-uniformly distributed large micelle and probably randomly distributed inclusion complex (100 nm scale) 5) Large vesicular aggregate of diameter around 251 nm consisting β-Cyclodextrin+ [BMPy][LS] IC (50 nm scale resolution) 6) Some more unique morphology of the Inclusion complex, which further justified size obtained by the Dynamic light scattering. On careful observation

homogenously distributed micellar aggregates also observable (around the big cluster).

4.4.9. Table of inclusion complexes of some C12 surfactant and Cyclodextrin and comparison between them:

Compound(Host)	Compound(Guest)	Techniques	Parameters obtained	Presence of 2:1 inclusion(Host: Guest)
β-Cyclodextrin	Bis- (dodecyl dimethylammonium) diethyl ether dibromide. This is a C-12 gemini surfactant.	^{1}H NMR, DOSY, ROESY	Aggregation number, Binding constant, Self-diffusion Coefficients [70]	Yes
β-Cyclodextrin	1-dodecyl-3-methylimidazolium hexafluorophosphate	Surface tension, FT-IR, XRD, NMR, 2D ^{1}H-^{1}H COSY, TGA	Crystal structure, Thermal stability, mode of inclusion and its mechanism [71]	Yes
β-Cyclodextrin	Sodium dodecyl sulfate(SDS)	surfactant-selective electrodes	Binding constant [72]	Yes
α-Cyclodextrin	Sodium dodecyl sulfate(SDS)	surfactant-selective electrodes	Binding constant [72]	Yes
α-Cyclodextrin	dodecyltrimethylammonium bromide	surfactant-selective electrodes	Binding constant [72]	No
β-Cyclodextrin	dodecyltrimethylammonium bromide	surfactant-selective electrodes	Binding constant [72]	No

4.5 Conclusion

From the spectroscopic studies (FTIR, NMR, and Mass), it is confirmed that the synthesized ionic liquid-based surfactant was 1-butyl-4-methylpyridinium lauryl sulfate. It can be used as a fluorescence quencher, a benign & efficient surfactant. Further, in the presence of β-cyclodextrin, it becomes more efficient surfactant which was confirmed by the critical studies of micellization. Conductivity, surface tension, and fluorescence study confirms the formation of a well fitted 1:1 host-guest as well as unique 2:1 inclusion complex with β-cyclodextrin. From the UV-Vis job plot and HRTEM, the formation of the mixed inclusion complexes was undoubtedly established. The HRTEM also had given unique morphology of the inclusion complex along with the simultaneous presence of both micelle and vesicle which was further supported by Dynamic light scattering result. Therefore this work and

novel data from this work may give a new insight of molecular interaction, supramolecular delivery system, and much more applications.

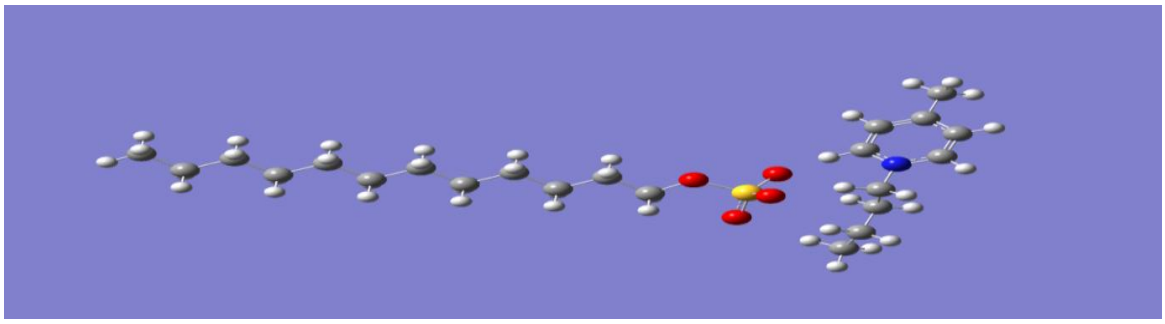

Scheme 1: Optimized 3D structure of the [BMPy] [LS]

Table S. 1: Data for the graph of CMC determination by conductance vs. conc. of [BMPy] [LS]

Volume(mL)	Total volume(mL)	Conc.(mM)	Cond. (µS/ppm)	Cond.(µScm^{-1})
0	15	0	4.59	41.73
0.3	15.3	0.196	9.8	89.09
0.6	15.6	0.385	14.1	128.2
0.9	15.9	0.566	25	227.3
1.2	16.2	0.741	34.4	312.7
1.5	16.5	0.909	46.6	423.6
1.8	16.8	1.071	54	490.9
2.1	17.1	1.228	60.7	551.8
2.4	17.4	1.379	69.6	632.7
2.7	17.7	1.525	73.4	667.3
3	18	1.667	79.1	719.1
3.3	18.3	1.803	84.8	770.9
3.6	18.6	1.935	88.3	802.7
3.9	18.9	2.063	91	827.3
4.2	19.2	2.188	94	854.5
4.5	19.5	2.308	99	900
4.8	19.8	2.424	103	936.4
5.1	20.1	2.537	106	963.6
5.4	20.4	2.647	110	1000
5.7	20.7	2.754	112	1018
6	21	2.857	112	1018

Volume(mL)	Total volume(mL)	Conc.(mM)	Cond. (µS/ppm)	Cond.(µScm^{-1})
6.3	21.3	2.958	120	1091
6.6	21.6	3.056	119	1082
6.9	21.9	3.151	121	1100
7.2	22.2	3.243	122	1109
7.5	22.5	3.333	123	1118
7.8	22.8	3.421	126	1145
8.1	23.1	3.506	127	1155
8.4	23.4	3.59	128	1164
8.7	23.7	3.671	135	1227
9	24	3.75	135	1227

Table S. 2: Data for the graph of breakpoint determination by conductance of [BMPy][LS] vs. conc. β- cyclodextrin (Host & Guest)

Vol. added(mL)	Cond. (mSCm^{-1})	Conc. (mM)	Total vol. (mL)	Cond. (mSCm^{-1})	Conc. (mM)
0	0.554	0	10	5.036	0
0.5	0.544	0.048	10.5	4.945	0.476
1	0.536	0.091	11	4.873	0.909
1.5	0.529	0.13	11.5	4.809	1.304
2	0.518	0.167	12	4.709	1.667
2.5	0.494	0.2	12.5	4.491	2
3	0.474	0.231	13	4.309	2.308
3.5	0.45	0.259	13.5	4.091	2.593
4	0.423	0.286	14	3.845	2.857
4.5	0.406	0.31	14.5	3.691	3.103
5	0.391	0.333	15	3.555	3.333
5.5	0.376	0.355	15.5	3.418	3.548
6	0.362	0.375	16	3.291	3.75
6.5	0.35	0.394	16.5	3.182	3.939
7	0.336	0.412	17	3.055	4.118
7.5	0.326	0.429	17.5	2.964	4.286
8	0.313	0.444	18	2.845	4.444
8.5	0.305	0.459	18.5	2.773	4.595
9	0.296	0.474	19	2.691	4.737
9.5	0.286	0.487	19.5	2.6	4.872
10	0.278	0.5	20	2.527	5

Vol. added(mL)	Cond. ($mSCm^{-1}$)	Conc. (mM)	Total vol. (mL)	Cond. ($mSCm^{-1}$)	Conc. (mM)
10.5	0.27	0.512	20.5	2.455	5.122
11	0.259	0.524	21	2.355	5.238
11.5	0.254	0.535	21.5	2.309	5.349
12	0.246	0.545	22	2.236	5.455
12.5	0.24	0.556	22.5	2.182	5.556
13	0.236	0.565	23	2.145	5.652
13.5	0.229	0.574	23.5	2.082	5.745
14	0.223	0.583	24	2.027	5.833
14.5	0.219	0.592	24.5	1.991	5.918
15	0.216	0.6	25	1.964	6
15.5	0.21	0.608	25.5	1.909	6.078
16	0.206	0.615	26	1.873	6.154
16.5	0.201	0.623	26.5	1.827	6.226
17	0.194	0.63	27	1.764	6.296
17.5	0.194	0.636	27.5	1.764	6.364
18	0.189	0.643	28	1.718	6.429
18.5	0.185	0.649	28.5	1.682	6.491
19	0.182	0.655	29	1.655	6.552
19.5	0.178	0.661	29.5	1.618	6.61
20	0.174	0.667	30	1.582	6.667
20.5	0.169	0.672	30.5	1.536	6.721
21	0.168	0.677	31	1.527	6.774
21.5	0.164	0.683	31.5	1.491	6.825
22	0.162	0.688	32	1.473	6.875
22.5	0.159	0.692	32.5	1.445	6.923
23	0.156	0.697	33	1.418	6.97
23.5	0.154	0.701	33.5	1.4	7.015
24	0.154	0.706	34	1.4	7.059
24.5	0.15	0.71	34.5	1.364	7.101
25	0.148	0.714	35	1.345	7.143
25.5	0.145	0.718	35.5	1.318	7.183
26	0.143	0.722	36	1.3	7.222
26.5	0.142	0.726	36.5	1.291	7.26
27	0.139	0.73	37	1.264	7.297
27.5	0.137	0.733	37.5	1.245	7.333
28	0.135	0.737	38	1.227	7.368

Vol. added(mL)	Cond. ($mSCm^{-1}$)	Conc. (mM)	Total vol. (mL)	Cond. ($mSCm^{-1}$)	Conc. (mM)
28.5	0.133	0.74	38.5	1.209	7.403
29	0.131	0.744	39	1.191	7.436
29.5	0.128	0.747	39.5	1.164	7.468
30	0.128	0.75	40	1.164	7.5
30.5	0.126	0.753	40.5	1.145	7.531
31	0.124	0.756	41	1.127	7.561
31.5	0.123	0.759	41.5	1.118	7.59
32	0.121	0.762	42	1.1	7.619
32.5	0.119	0.765	42.5	1.082	7.647
33	0.117	0.767	43	1.064	7.674
33.5	0.117	0.77	43.5	1.064	7.701
34	0.116	0.773	44	1.055	7.727
34.5	0.115	0.775	44.5	1.045	7.753
35	0.114	0.778	45	1.036	7.778
35.5	0.112	0.78	45.5	1.018	7.802
36	0.111	0.783	46	1.009	7.826
36.5	0.108	0.785	46.5	0.982	7.849
37	0.108	0.787	47	0.982	7.872
37.5	0.108	0.789	47.5	0.982	7.895
38	0.107	0.792	48	0.973	7.917
38.5	0.105	0.794	48.5	0.955	7.938
39	0.106	0.796	49	0.964	7.959
39.5	0.105	0.798	49.5	0.955	7.98
40	0.104	0.286	14	0.945	2.857
40.5	0.103	0.802	50.5	0.936	8.02
41	0.101	0.804	51	0.918	8.039
41.5	0.101	0.806	51.5	0.918	8.058
42	0.101	0.808	52	0.918	8.077
42.5	0.099	0.81	52.5	0.9	8.095
43	0.098	0.811	53	0.891	8.113
43.5	0.098	0.813	53.5	0.891	8.131
44	0.097	0.815	54	0.882	8.148
44.5	0.096	0.817	54.5	0.873	8.165
45	0.095	0.818	55	0.864	8.182
45.5	0.093	0.82	55.5	0.845	8.198
46	0.093	0.821	56	0.845	8.214

Vol. added(mL)	Cond. ($mSCm^{-1}$)	Conc. (mM)	Total vol. (mL)	Cond. ($mSCm^{-1}$)	Conc. (mM)
46.5	0.093	0.823	56.5	0.845	8.23
47	0.092	0.825	57	0.836	8.246
47.5	0.092	0.826	57.5	0.836	8.261
48	0.091	0.828	58	0.827	8.276
48.5	0.089	0.829	58.5	0.809	8.291
49.5	0.089	0.998	59	0.809	9.98
50	0.088	0.833	60	0.8	8.333

Table S. 3. Data for the CMC determination of [BMPy][LS] by surface tension

Volume added (mL)	Total volume (mL)	Conc.(mM)	log(Conc.)	S.T.(mNM^{-1})
0	10	0	0	72.6
0.3	10.3	0.262	-0.58	55.6
0.6	10.6	0.509	-0.29	47.6
0.9	10.9	0.743	-0.13	44
1.2	11.2	0.964	-0.02	41.6
1.5	11.5	1.174	0.07	39.2
1.8	11.8	1.373	0.138	37.6
2.1	12.1	1.562	0.194	36.7
2.4	12.4	1.742	0.241	36.8
2.7	12.7	1.913	0.282	37
3	13	2.077	0.317	37.3
3.3	13.3	2.233	0.349	37.3
3.6	13.6	2.382	0.377	37.5
3.9	13.9	2.525	0.402	37.2
4.2	14.2	2.662	0.425	37.4
4.5	14.5	2.793	0.446	37.7
4.8	14.8	2.919	0.465	37.9
5.1	15.1	3.04	0.483	37.9
5.4	15.4	3.156	0.499	37.6
5.7	15.7	3.268	0.514	37.5
6	16	3.375	0.528	38
6.3	16.3	3.479	0.541	37.9

Table S. 4. Data for the breakpoint determination of [BMPy][LS] by surface ST (IC)

Vol. added(mL)	Total volume(mL)	Conc.(mM)	S.T.(mNm-1)
0	10	0	36.9
0.43	10.43	0.206	36.1
0.86	10.86	0.396	36.2
1.29	11.29	0.571	36.4
1.72	11.72	0.734	35.3
2.15	12.15	0.885	35.1
2.58	12.58	1.025	34.4
3.01	13.01	1.157	34.6
3.44	13.44	1.28	34.3
3.87	13.87	1.395	34.4
4.30	14.30	1.5035	34.8
4.73	14.73	1.606	33.4
5.16	15.16	1.702	34.2
5.59	15.59	1.793	33.5
6.02	16.02	1.879	34.2
6.45	16.45	1.960	34.7
6.88	16.88	2.038	34.3
7.31	17.31	2.112	36.7
7.74	17.74	2.182	38.1
8.17	18.17	2.248	38.0
8.60	18.6	2.3118	37.8
9.03	19.03	2.373	40.5
9.46	19.46	2.431	43.3
9.89	19.89	2.486	45.3
10.32	20.32	2.539	47.7
10.75	20.75	2.59	47.9
11.18	21.18	2.639	47.5
11.61	21.61	2.686	49.1
12.04	22.04	2.731	50
12.47	22.47	2.775	50.4
12.90	22.90	2.817	50.4

Table S. 5: Data for the Job plot performed by UV-Vis spectroscopy for aqueous [BMPy][LS] -β-CD system at 298.15K[a](252 nm)

β-CD (mL)	G (mL)	β-CD (µM)	G (µM)	Mole fraction (R)	Abs. (A)	Abs. diff ΔA	R* ΔA R* ΔA
0	2	0.0	100	1	0.32215	0.0	0.0
0.2	1.8	10	90	0.9	0.29185	0.0303	0.02727

0.4	1.6	20	80	0.8	0.25945	0.0627	0.05016
0.6	1.4	30	70	0.7	0.23135	0.0908	0.06356
0.8	1.2	40	60	0.6	0.19704	0.12511	0.07507
1	1	50	50	0.5	0.16333	0.15882	0.07941
1.2	0.8	60	40	0.4	0.13379	0.18836	0.07534
1.4	0.6	70	30	0.3	0.09963	0.22252	0.06676
1.6	0.4	80	20	0.2	0.06104	0.26111	0.05222
1.8	0.2	90	10	0.1	0.031	0.29115	0.02911
2	0.0	100	0	0.0	-0.00151	0.32366	0.0

[a] Standard uncertainties in temperature are = ±0.01 K.

[b] **G**=Guest **(**[BMPy][LS]**)**

Table S. 6: Data for the Job plot performed by UV-Vis spectroscopy for aqueous [BMPy][LS]-β-CD system at 298.15K(220 nm)

β-CD (mL)	G (mL)	β-CD (µM)	G (µM)	Mole fraction (R)	Abs. (A)	Abs. diff ΔA	R* ΔA R* ΔA
0.0	2	0	100	1	0.75879	0.0	0.0
0.2	1.8	10	90	0.9	0.68509	0.0737	0.06633
0.4	1.6	20	80	0.8	0.6121	0.14669	0.11735
0.6	1.4	30	70	0.7	0.54767	0.21112	0.14778
0.8	1.2	40	60	0.6	0.46897	0.28982	0.17389
1	1	50	50	0.5	0.39154	0.36725	0.18362
1.2	0.8	60	40	0.4	0.32064	0.43815	0.17526
1.4	0.6	70	30	0.3	0.23932	0.51947	0.15584

1.6	0.4	80	20	0.2	0.15116	0.60763	0.12153
1.8	0.2	90	10	0.1	0.07512	0.68367	0.06837
2	0.0	100	0	0	-0.00108	0.75987	0.0

[a] Standard uncertainties in temperature are = ±0.01 K.

[b] **G**=Guest **(**[BMPy][LS]**)**

Table S. 7: Data for Refractive Index

Conc.(mM) ([BMPy][LS])	Conc.(mM) (β -CD)	Temperature(K)	RI values
0.0	5	293.15	1.3324
0.16	1.83		1.3323
0.33	1.66		1.3323
0.55	1.5		1.3323
0.66	1.33		1.3322
0.83	1.16		1.3323
1	1		1.3322
1.16	0.83		1.3322
1.33	0.66		1.3323
1.5	0.55		1.3323
1.66	0.33		1.3324
1.83	0.16		1.3322
5	0.0		1.3324

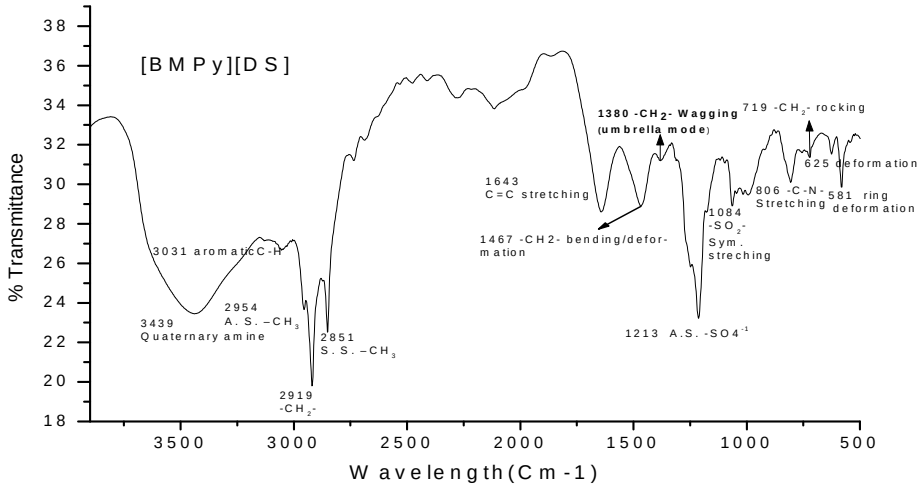

Fig. S. 1. a) FTIR spectra of 1-butyl-4-methylpyridinium lauryl sulfate in KBr pellets

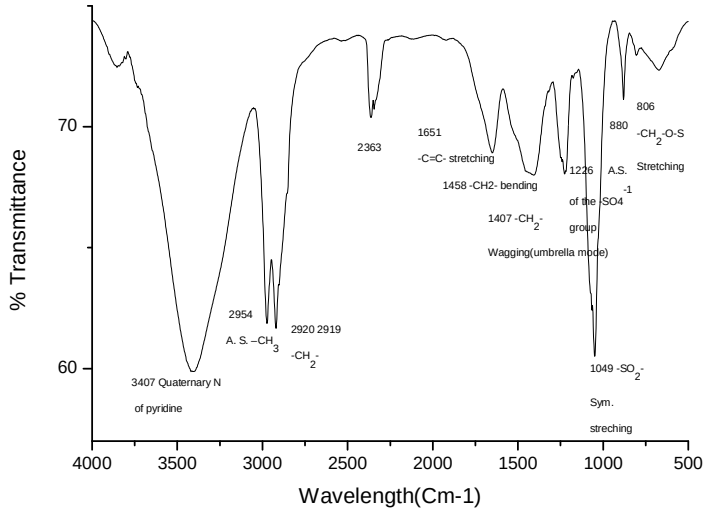

Fig. S. 1. b) FTIR spectra of 1-butyl-4-methylpyridinium lauryl sulfate in EtOH

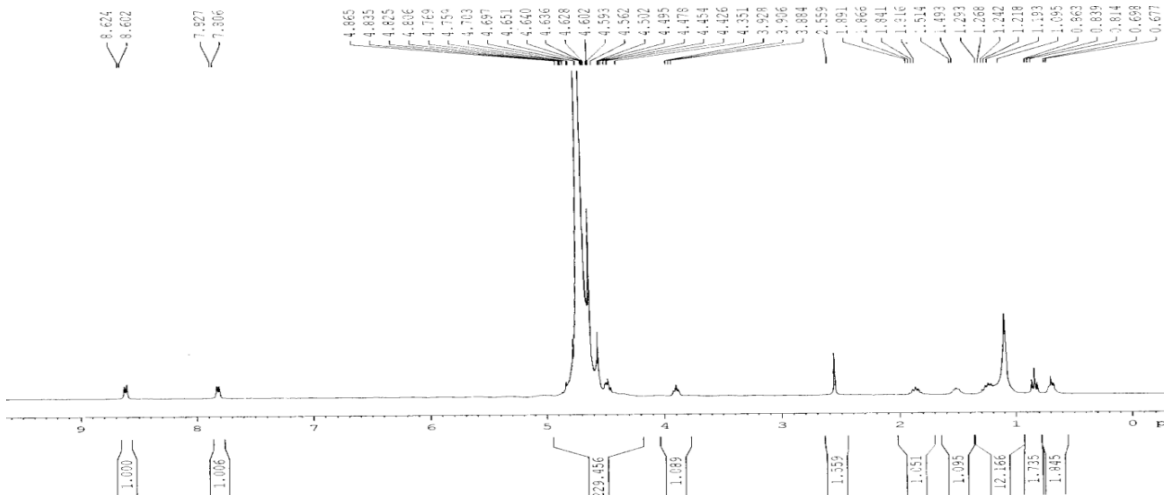

Fig. S. 2a. NMR spectra of 1-butyl-4-methylpyridinium lauryl sulphate in D_2O

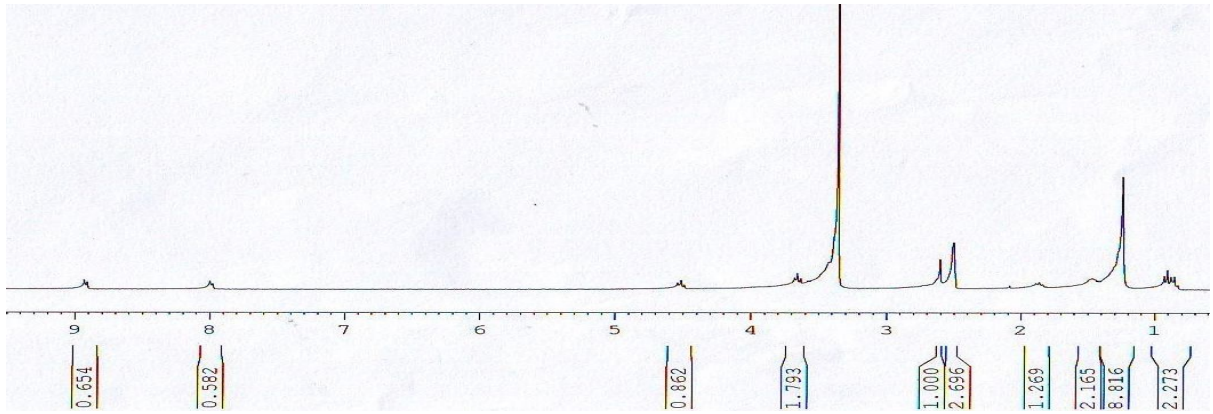

Fig. S. 2b. NMR Spectra of 1-Butyl-4-methylpyridinium lauryl sulphate in DMSO-d_6

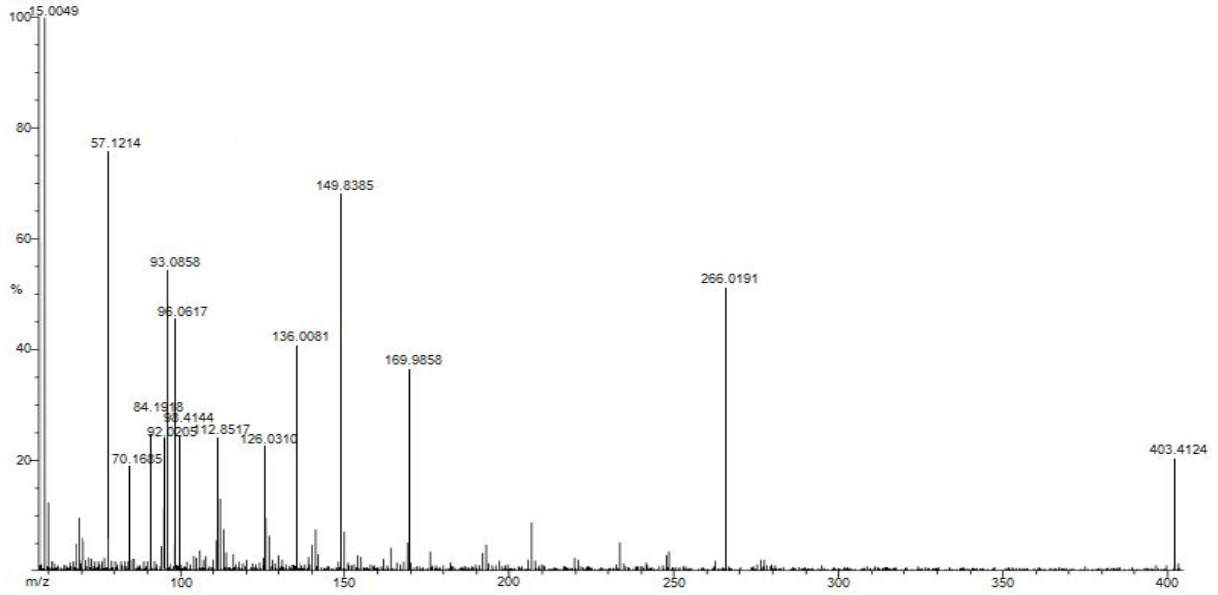

Fig. S. 3 Mass spectrum of 1-butyl-4-methylpyridinium lauryl sulfate

Table S. 8. ^{1}H NMR data of ([BMPy][LS]), β-CD and their inclusion complexes

[BMPy][LS] (300MHz, Solvent: D_2O) δ /ppm	
^{1}H NMR (**300** MHz, **D_2O**): δ 8.60-8.62(d, 2H, *J*=6.6 Hz) $N(CH)_2$ of pyridinium ring, 7.80-7.83(d, 2H, *J*=6.3 Hz) $N^+CC(CH)_2$ of pyridinium ring, 4.48(t, 2H, NCH_2), 3.89(t, 2H, $SOCH_2$), 2.55 (s, 3H, -CH_3 para to N), 1.86 (m, 2H, $NCCH_2$), 1.55 (t, 2H, $NCCCH_2$), 1.21 (m, $SOCH_2(CH_2)_9$, 20H), 0.80(m,3H, $NCCCCH_3$), 0.68(m,3H, $SOC_{11}CH_3$).	
β-CD (400 MHz, Solvent: D_2O), δ /ppm	β-CD+[BMPy][LS] (400 MHz, Solvent: D_2O), δ /ppm
3.49-3.54 (H4, 7H, t, *J* = 9.2 Hz), 3.57-3.60 (H2, 7H, dd, *J* = 9.6, 3.2 Hz), 3.79-3.84 (H6, H5, 14H, m), 3.87-3.92 (H3, 7H, t, *J* = 9.2 Hz), 5.00-5.01 (H1, 7H, d, *J* = 3.6 Hz).	8.47-8.46(d, 2H) included $N(CH)_2$ of pyridinium ring, 7.68-7.7(d, 2H) included $N^+CC(CH)_2$ of pyridinium ring, 4.92-4.9(H1, 7H , d), 4.69(s) suppressed, 4.34-4.37(t, 2H, NCH_2), 3.88-3.9(t), 3.68-3.76(m), 3.53-3.55(dd), 3.46-3.49(t), 1.79-1.83(m), 1.49-1.56(m), 1.14-1.22(m), 1.11(s), 0.75- 0.8(m).
Shift of δ /ppm in β-cyclodextrin	Shift of δ /ppm in ([BMPy][LS])
H3, H5 showed up field shift. H1, H2 & H4, H6 show considerable shift which	Both 8.60-8.62(d, 2H)$N(CH)_2$, 7.80-7.83(d, 2H) $N^+CC(CH)_2$ of pyridine

prove inclusion for both. Shift of H6 prove 2:1 inclusion.	undergo up field shift due to its inclusion into the β–Cyclodextrin cavity. Alkyl chain of pyridine 4.48(t, 2H, NCH_2) also undergo up field shift for the previously mentioned reason.

β-CD+[BMPy][LS] inclusion complex 1H NMR after few months (400 MHz, Solvent: D_2O), δ /ppm

8.457-8.440(d, 2H, included $N(CH)_2$ of pyridinium ring), 7.682-7.667(d, 2H, included $N^+CC(CH)_2$ of pyridinium ring), 4.902-4.893, 4.361-4.324(t), 3.905-3.873(t),

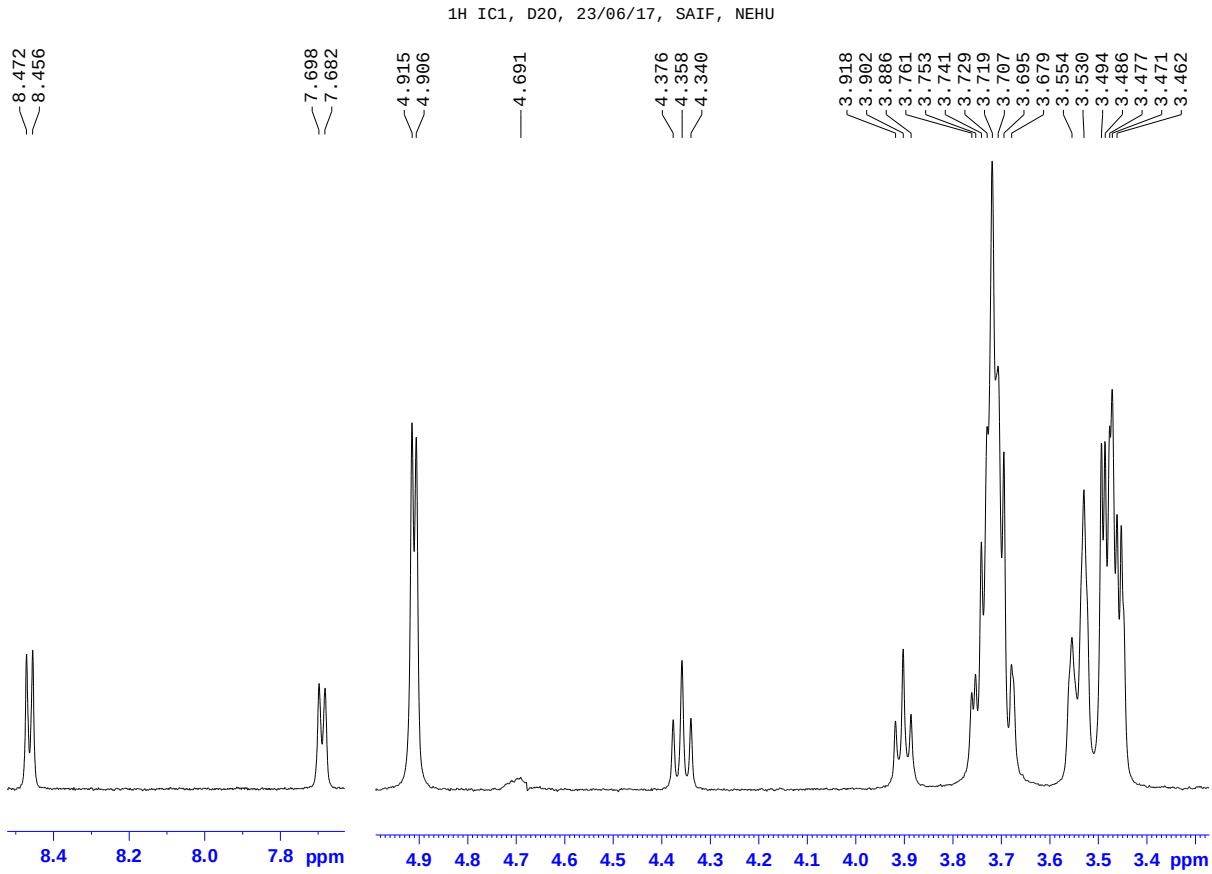

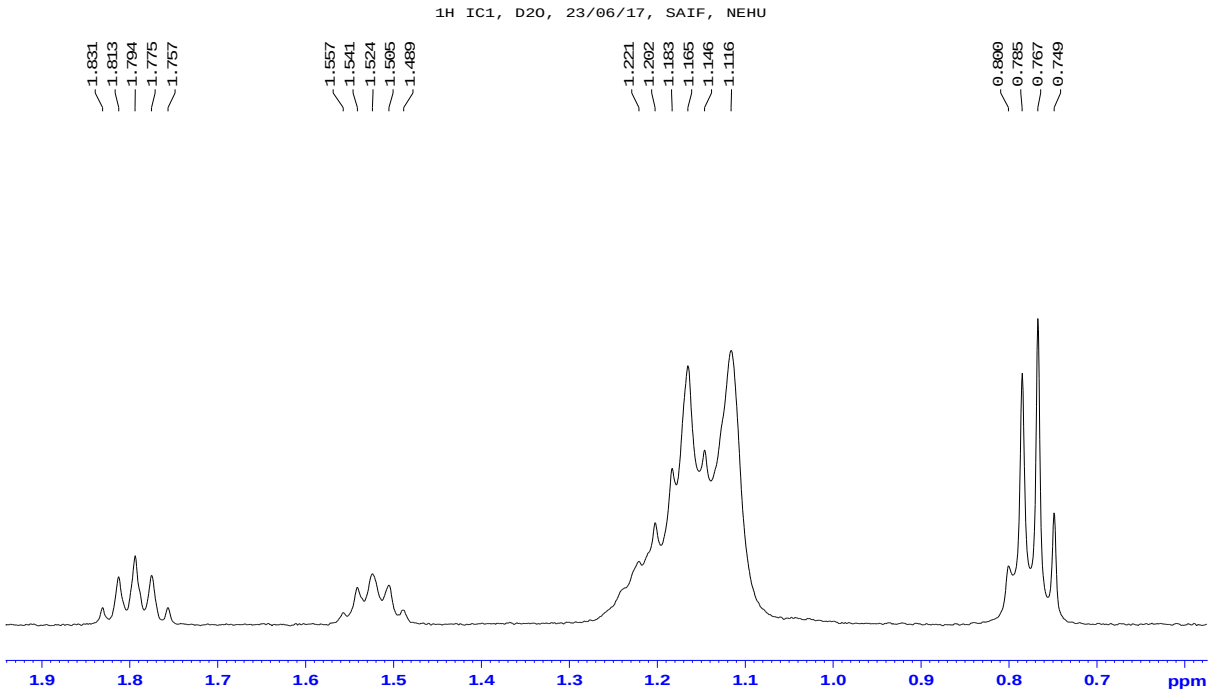

Fig S. 4. a) & b) The NMR spectra of inclusion complex consisting 1-butyl-4-methylpyridinium lauryl sulphate & β –CD in D_2O.

Table S.9. Source and purity of the chemicals

Chemical name	CAS number	Source	mass fraction purity	Purification method
BMPyCl	112400-86-9	Aldrich	>0.990	Used as procured
SLS	151-21-3	Merck	>0.980	Used as procured
D_2O	7789-20-0	Aldrich	>0.999	Used as procured
Pyrene	129-00-0	Fluka	>0.990	Used as procured
β-CD	7585-39-9	Aldrich	>0.990	Used as procured
DMSO-d_6	2206-271	SRL	>0.998	Used as procured

Table: S.10 Hydrodynamic diameter (Dh) and PDI values of β-CD, [BMPy][LS], systems in water obtained by DLS studies.

Parameter	β-CD	β-CD	β-CD IC	β-CD IC	β-CD IC	β-CD IC	B-CD IC
Hydrodynamic diameter (nm)	183.7	119.7	294.3	248.5	294.8	209.5	256
PDI	0.58	0.312	0.701	0.708	0.788	0.64	0.655

Fig.S.5:

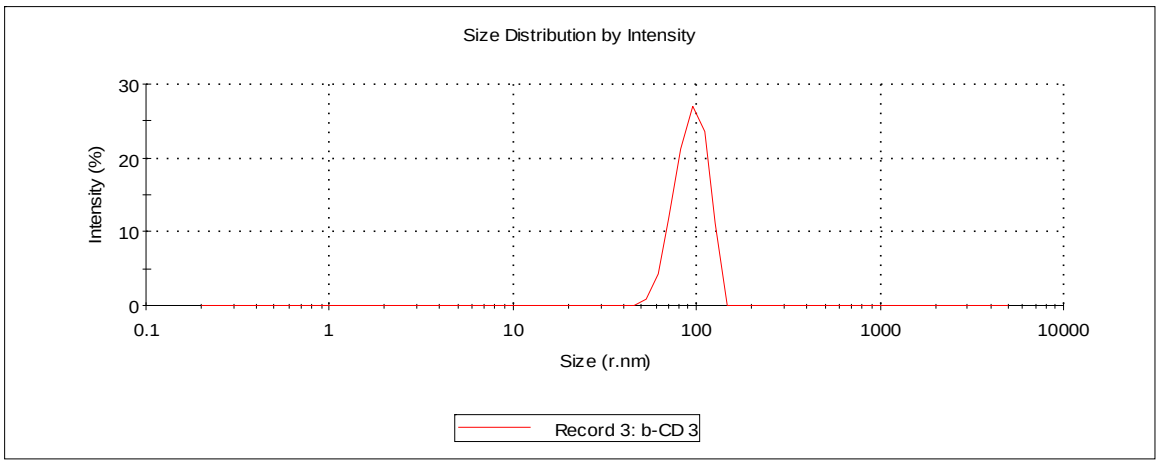

(a) A representive Intensity vs. Size distribution graph for the β-CD

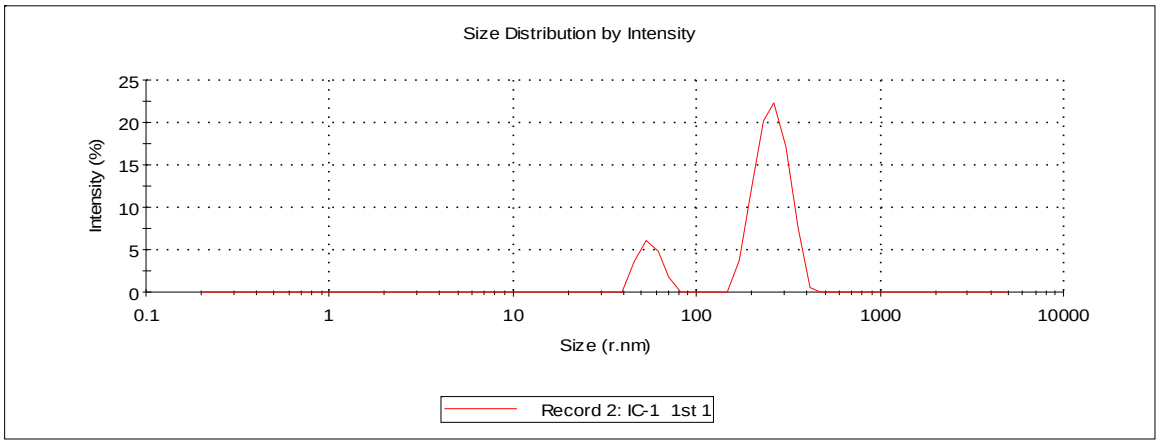

(b) A representive Intensity vs. Size distribution graph for the [BMPy][LS]

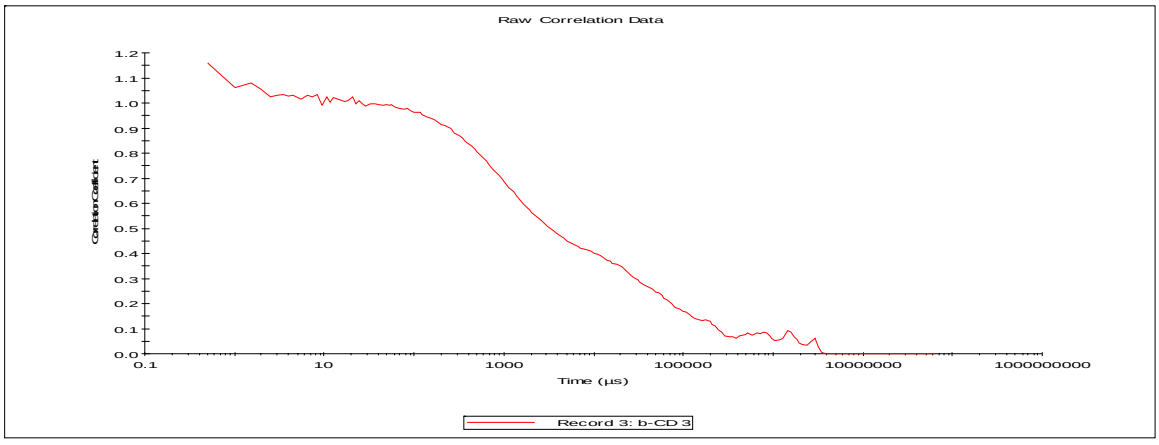

(c) One of the few Correlagram of β-CD.

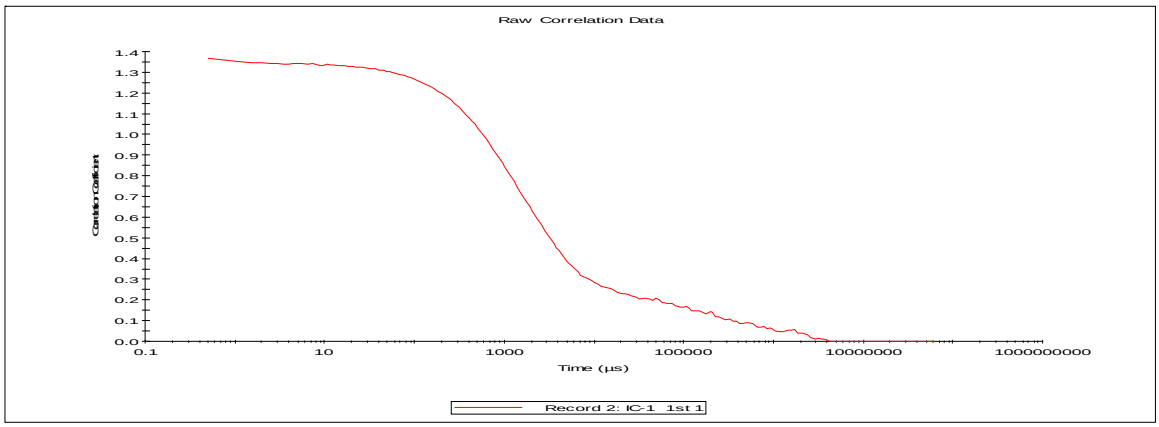

(d) One of the few Correlagram of [BMPy][LS]